UPPSALA
UNIVERSITET

Digital Comprehensive Summaries of Uppsala Dissertations from the Faculty of Science and Technology 1719

Electron energization in near-Earth space

Studies of kinetic scales using multi-spacecraft data

ELIN ERIKSSON

ACTA
UNIVERSITATIS
UPSALIENSIS
UPPSALA
2018

ISSN 1651-6214
ISBN 978-91-513-0437-3
urn:nbn:se:uu:diva-359594

Dissertation presented at Uppsala University to be publicly examined in Polhemsalen, Ångström Laboratory 10134, Lägerhyddsvägen 1, Uppsala, Thursday, 25 October 2018 at 10:00 for the degree of Doctor of Philosophy. The examination will be conducted in English. Faculty examiner: Professor Masahiro Hoshino (University of Tokyo).

Abstract

Eriksson, E. 2018. Electron energization in near-Earth space. Studies of kinetic scales using multi-spacecraft data. *Digital Comprehensive Summaries of Uppsala Dissertations from the Faculty of Science and Technology* 1719. 80 pp. Uppsala: Acta Universitatis Upsaliensis. ISBN 978-91-513-0437-3.

Plasma, a gas of charged particles exhibiting collective behavior, is everywhere in the Universe. The heating of plasma to millions of degrees and acceleration of charged particles to very high energies has been observed in many astrophysical environments. How and where the heating and acceleration occur is in many cases unclear. In most astrophysical environments, plasma consists of negative electrons and positive ions. In this thesis we focus on understanding the heating and acceleration of electrons. Several plasma processes have been proposed to explain the observed acceleration. However, the exact heating and acceleration mechanisms involved and their importance are still unclear. This thesis contributes toward a better understanding of this topic by using observations from two multi-spacecraft missions, Cluster and the Magnetospheric MultiScale (MMS), in near-Earth space.

In Article I we look at magnetic nulls, regions of vanishing magnetic field **B** believed to be important in particle acceleration, in the Earth's nightside magnetosphere. We find that nulls are common at the nightside magnetosphere and that the characterization of the **B** geometry around a null can be affected by localized **B** fluctuations. We develop and present a method for determining the effect of the **B** fluctuation on the null's characterization.

In Article II we look at a thin (a few km) current sheet (CS) in the turbulent magnetosheath. Observations suggest local electron heating and beam formation parallel to **B** inside the CS. The electron observations fits well with the theory of electron acceleration across a shock due to a potential difference. However, in our case the electron beams are formed locally inside the magnetosheath that is contrary to current belief that the beam formation only occurs at the shock.

In Article III we present observations of electron energization inside a very thin (thinner than Article II) reconnecting CS located in the turbulent magnetosheath. Currently, very little is know about electron acceleration mechanisms at these small scales. MMS observe local electron heating and acceleration parallel to **B** when crossing the CS. We show that the energized electrons correspond to acceleration due to a quasi-static potential difference rather than electrostatic waves. This energization is similar to what has been observed inside ion diffusion regions at the magnetopause and magnetotail. Thus, despite the different plasma conditions a similar energization occurs in all these plasma regions.

In Article IV we study electron acceleration by Fermi acceleration, betatron acceleration, and acceleration due to parallel electric fields inside tailward plasma jets formed due to reconnection, the so called tailward outflow region. We show that most observations are consistent with local electron heating and acceleration from a simplified two dimensional picture of Fermi acceleration and betatron acceleration in an outflow region. We find that Fermi acceleration is the dominant electron acceleration mechanism.

Keywords: magnetic reconnection, electron acceleration, electron heating, magnetosheath, magnetotail, magnetic nulls, Cluster, Magnetospheric MultiScale

Elin Eriksson, Swedish Institute of Space Physics, Uppsala Division, Box 537, Uppsala University, SE-75121 Uppsala, Sweden. Department of Physics and Astronomy, Box 516, Uppsala University, SE-751 20 Uppsala, Sweden.

ISSN 1651-6214
ISBN 978-91-513-0437-3
urn:nbn:se:uu:diva-359594 (http://urn.kb.se/resolve?urn=urn:nbn:se:uu:diva-359594)

To my parents
Kerstin and Per Ola

List of Articles

This thesis is based on the following articles, which are referred to in the text by their Roman numerals. All reprints are made with permission from the respective publishers.

I *Statistics and accuracy of magnetic null identification in multispacecraft data*

E. Eriksson, A. Vaivads, Yu. V. Khotyaintsev, V. M. Khotyayintsev, and M. André
Geophysical Research Letters, Volume 42, Issue 17, 2015, Pages 7
DOI:10.1002/2015GL064959

II *Strong current sheet at a magnetosheath jet: Kinetic structure and electron acceleration*

E. Eriksson, A. Vaivads, D. B. Graham, Yu. V. Khotyaintsev, E. Yordanova, H. Hietala, M. André, L. A. Avanov, J. C. Dorelli, D. J. Gershman, B. L. Giles, B. Lavraud, W. R. Paterson, C. J. Pollock, Y. Saito, W. Magnes, C. Russell, R. Torbert, R. Ergun, P- A. Lindqvist, and J. Burch
Journal of Geophysical Research: Space Physics, Volume 121, Issue 10, 2016, Pages 11
DOI:10.1002/2016JA023146

III *Electron Energization at a Reconnecting Magnetosheath Current Sheet*

E. Eriksson, A. Vaivads, D. B. Graham, A. Divin, Yu. V. Khotyaintsev, E. Yordanova, M. André, B. L. Giles, C. J. Pollock, C. Russell, O. Le Contel, R. Torbert, R. Ergun, P- A. Lindqvist, and J. Burch
Geophysical Research Letters, Volume 45, Issue 16, 2018, Pages 10
DOI:10.1029/2018GL078660

IV *Electron acceleration in a magnetotail reconnection outflow region using Magnetospheric MultiScale data*

E. Eriksson, A. Vaivads, L. Alm, D. B. Graham, Yu. V. Khotyaintsev, and M. André,
Manuscript in preparation

Articles not included in the thesis

Olshevsky, V., A. Divin, **E. Eriksson**, S. Markidis, and G. Lapenta (2015). "Energy Dissipation in Magnetic Null Points at Kinetic Scales". *The Astrophysical Journal* 807.
DOI: 10.1088/0004-637X/807/2/155.

Khotyaintsev, Y. V., D. B. Graham, C. Norgren, **E. Eriksson**, W. Li, A. Johlander, A. Vaivads, M. André, P. L. Pritchett, A. Retinò, T. D. Phan, R. E. Ergun, K. Goodrich, P.-A. Lindqvist, G. T. Marklund, O. Le Contel, F. Plaschke, W. Magnes, R. J. Strangeway, C. T. Russell, H. Vaith, M. R. Argall, C. A. Kletzing, R. Nakamura, R. B. Torbert, W. R. Paterson, D. J. Gershman, J. C. Dorelli, L. A. Avanov, B. Lavraud, Y. Saito, B. L. Giles, C. J. Pollock, D. L. Turner, J. D. Blake, J. F. Fennell, A. Jaynes, B. H. Mauk, and J. L. Burch (2016). "Electron jet of asymmetric reconnection". *Geophysical Research Letters* 43.
DOI: 10.1002/2016GL069064.

Yordanova, E., Z. Vörös, A. Varsani, D. B. Graham, C. Norgren, Y. V. Khotyaintsev, A. Vaivads, **E. Eriksson**, R. Nakamura, P.-A. Lindqvist, G. Marklund, R. E. Ergun, W. Magnes, W. Baumjohann, D. Fischer, F. Plaschke, Y. Narita, C. T. Russell, R. J. Strangeway, O. Le Contel, C. Pollock, R. B. Torbert, B. J. Giles, J. L. Burch, L. A. Avanov, J. C. Dorelli, D. J. Gershman, W. R. Paterson, B. Lavraud, and Y. Saito (2016). "Electron scale structures and magnetic reconnection signatures in the turbulent magnetosheath". *Geophysical Research Letters* 43.
DOI: 10.1002/2016GL069191.

Chasapis, A., W. H. Matthaeus, T. N. Parashar, O. Le Contel, A. Retinò, H. Breuillard, Y. Khotyaintsev, A. Vaivads, B. Lavraud, **E. Eriksson**, T. E. Moore, J. L. Burch, R. B. Torbert, P.-A. Lindqvist, R. E. Ergun, G. Marklund, K. A. Goodrich, F. D. Wilder, M. Chutter, J. Needell, D. Rau, I. Dors, C. T. Russell, G. Le, W. Magnes, R. J. Strangeway, K. R. Bromund, H. K. Leinweber, F. Plaschke, D. Fischer, B. J. Anderson, C. J. Pollock, B. L. Giles, W. R. Paterson, J. Dorelli, D. J. Gershman, L. Avanov, and Y. Saito (2017). "Electron Heating at Kinetic Scales in Magnetosheath Turbulence". *The Astrophysical Journal* 836.
DOI: 10.3847/1538-4357/836/2/247.

Oka, M., J. Birn, M. Battaglia, C. C. Chaston, S. M. Hatch, G. Livadiotis, S. Imada, Y. Miyoshi, M. Kuhar, F. Effenberger, **E. Eriksson**, Y. V. Khotyaintsev, and A. Retinò (2018). "Electron Power-Law Spectra in Solar and Space Plasmas". *Space Science Reviews* 214.
DOI: 10.1007/s11214-018-0515-4.

Vörös, Z., E. Yordanova, A. Varsani, K. J. Genestreti, Y. V. Khotyaintsev, W. Li, D. B. Graham, C. Norgren, R. Nakamura, Y. Narita, F. Plaschke, W. Magnes, W. Baumjohann, D. Fischer, A. Vaivads, **E. Eriksson**, P.-A. Lindqvist, G. Marklund, R. E. Ergun, M. Leitner, M. P. Leubner, R. J. Strangeway, O. Le Contel, C. Pollock, B. J. Giles, R. B. Torbert, J. L. Burch, L. A. Avanov, J. C. Dorelli, D. J. Gershman, W. R. Paterson, B. Lavraud, and Y. Saito (2017). "MMS Observation of Magnetic Reconnection in the Turbulent Magnetosheath". *Journal of Geophysical Research: Space Physics* 122. DOI: 10.1002/2017JA024535.

Fu, H. S., J. B. Cao, A. Vaivads, Y. V. Khotyaintsev, M. Andre, M. Dunlop, W. L. Liu, H. Y. Lu, S. Y. Huang, Y. D. Ma, and **E. Eriksson** (2016). "Identifying magnetic reconnection events using the FOTE method". *Journal of Geophysical Research: Space Physics* 121. DOI: 10.1002/2015JA021701.

Foreword

Thesis

This PhD thesis is partly based on "3D Magnetic Nulls and Regions of Strong Current in the Earth's Magnetosphere", Licentiate dissertation, Uppsala University, 2016, by Elin Eriksson.

Thesis Cover

The picture of the Earth's magnetosphere covering the front and back cover was created by the Orbit Visualization Tool (`https://ovt.irfu.se`).

Contents

1. Introduction

Plasma, a gas of charged particles exhibiting collective behavior, is everywhere in the Universe. The heating of plasma to millions of degrees and acceleration of charged particles to energies well above thermal energy has been observed in many astrophysical environments. How and where the plasma heating and acceleration occur is in many cases unclear. In most astrophysical environments plasma consists of negative electrons and positive ions. In this thesis we focus on understanding the heating and acceleration of electrons. The main observations we have from astrophysical environments such as solar flares (Chen et al., 2015; Petrosian, 2016) and supernovae remnants (Helder et al., 2012) come from electromagnetic radiation generated by accelerated electrons. Electron acceleration has been observed in-situ in near-Earth space inside the magnetosheath (e.g., Retinò et al., 2008), magnetotail (e.g., Chen et al., 2008), the magnetopause (e.g., Graham et al., 2014), at magnetic flux pileup regions, also referred to as dipolarization fronts (e.g., Fu et al., 2011; Birn et al., 2013; Turner et al., 2016), and at shocks (e.g., Feldman et al., 1983). Electron acceleration has also been observed at other planets such as Saturn (e.g., Masters et al., 2016), Mercury (e.g., Dewey et al., 2017), and Jupiter (e.g., Mauk et al., 2017). Several important plasma processes have been proposed to explain the observed acceleration such as reconnection current sheets (Birn et al., 2012), wave-particle interactions (Cairns and McMillan, 2005), turbulence (Retinò et al., 2008), and shocks (Feldman et al., 1983). However, the exact heating and acceleration mechanisms involved and their importance are still in many cases unclear. This thesis is a contribution towards a deeper understanding of electron heating and acceleration in plasma.

One fundamental energy conversion process thought to be important for accelerating and heating electrons is magnetic reconnection. Magnetic reconnection occurs almost everywhere where strong currents flow within plasmas and is a process that changes the magnetic topology allowing plasma to move between different magnetic field lines (Priest and Forbes, 2000; Priest, 2003; Birn and Priest, 2007). During the magnetic topology change, magnetic energy is converted into heating of the plasma and particle acceleration. Magnetic reconnection is widely studied in different astrophysical, simulation, and laboratory plasmas (e.g., Jovanovic et al., 2005; Paschmann et al., 2013; Arridge et al., 2016; Egedal et al., 2007; Yamada et al., 2010). Reconnection is of particular interest because it leads to large scale topological changes of the magnetic field allowing e.g., solar wind plasma to enter planetary magnetospheres. Electron acceleration resulting from magnetic reconnection has been

observed directly in the near-Earth space (e.g., Birn et al., 2012, and references therein) and indirectly for solar flares (e.g., Cargill et al., 2012). Several regions of viable acceleration related to reconnection have been proposed, such as different regions at the reconnection X-line (e.g., Hoshino et al., 2001), dipolarization fronts created when accelerated plasma from magnetotail reconnection collide with pre-existing plasma (e.g., Hoshino et al., 2001; Fu et al., 2013) and at magnetic islands (e.g., Drake et al., 2006; Pritchett, 2008; Hoshino, 2012; Drake et al., 2013). However, the experimental confirmation and relative importance of these regions is still in many cases unclear. In this thesis we expand the knowledge of electron acceleration related to reconnection by including studies from the magnetosheath, one relatively unexplored region for electron acceleration in near-Earth space, and the magnetotail. The magnetosheath is an especially interesting plasma regime because there the thermal energy is much larger than the magnetic energy, which occurs in many other astrophysical environments, such as supernovae remnants. We also look at magnetic structures thought to be important for reconnection.

Laboratory, near space, and astrophysical plasma environments cover a wide range of magnetic fields and plasma densities. Surprisingly, when looking at non-dimensional parameters, such as the ratio between thermal and magnetic energy, these environments can be very similar to each other (Vaivads et al., 2009), see Fig. 1.1. Therefore, a deeper understanding in one plasma environment can possibly lead to a better understanding in other plasma environments.

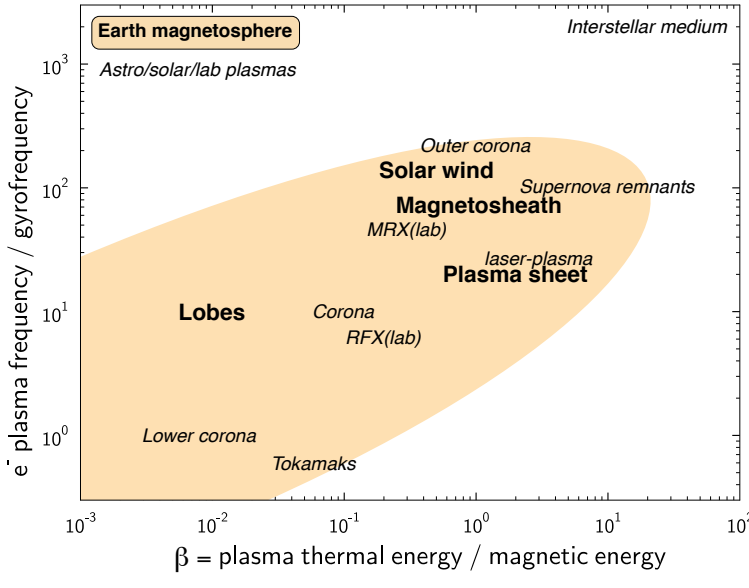

Figure 1.1. Many astrophysical and laboratory plasmas can be similar to near-Earth space when compared in non-dimensional parameter space. Adapted from Vaivads et al. (2009).

There are different advantages to studying plasma in a laboratory, near space, or astrophysical environment. The advantage of studying plasma in near-Earth space is the amount of detailed in-situ measurements of electric, magnetic fields, and particles; one can bring more instruments into the near-Earth space and therefore get more in-situ measurements back. The wealth of high-quality and high-resolution in-situ measurements is crucial to better determine the importance of different electron acceleration and heating mechanisms.

Despite the wealth of information from spacecraft, laboratory, and simulations understanding plasma is not easy. Both observational (laboratory and space) and simulation communities work together to try to understand what is happening in space. Simulations results are commonly compared with space observations, like in Article III. Powerful computer simulations can test out different theoretical models and conditions; a necessity when looking at processes occurring in large systems where the basic theory is too complicated to use. Furthermore, simulations allow us the possibility to explore other regions than just the small region crossed by the spacecraft.

In this thesis, we present four multi-spacecraft studies using data from the Cluster and **M**agnetospheric **M**ulti**S**cale (MMS) missions. In Article I we look at magnetic nulls, regions of vanishing magnetic field believed to be important in particle acceleration and reconnection, in the Earth's nightside magnetosphere. Article II is a kinetic study of a thin current sheet in the turbulent magnetosheath and its related electron acceleration. In Article III we look at a thin reconnecting magnetosheath current sheet and its associated electron energization and in Article IV we look at electron acceleration in an outflow region of magnetotail reconnection.

In the following chapters, we begin by giving a basic introduction to plasma physics, the terminology used in the articles, and the Earth's magnetosphere. We give a brief summary of magnetic reconnection and magnetic nulls. Thereafter, we give a short presentation of the Cluster and MMS missions, where we explain the function of the instruments used in articles I-IV and some of their limitations. After that we explain some important methods used in articles I-IV, including a magnetic null identification reliability method we created in Article I. Thereafter, an introduction to electron acceleration mechanisms, the main topic of this thesis, is given. In the last two chapters we discuss what the next steps of this research should be and give a summary of articles I-IV.

2. Basic Plasma Physics

In order to understand the detailed studies in articles I-IV some essential concepts needs to be introduced. Basic plasma physics is a wide subject and can be found in textbooks such as Chen (1974), Kivelson and Russell (1996), Baumjohann and Treumann (1996), Priest and Forbes (2000), Bellan (2006), and Kallenrode (2010). This chapter gives only a brief introduction to the most basic concepts of plasma that is of relevance to articles I-IV.

2.1 Plasma

When talking about matter, what usually comes to mind is gas, liquids, and solids. How we describe and manipulate these states has shaped how we scientifically view the world. If we look several Earth's radius Re [1] above the Earth's surface, almost all matter is ionized due to the electromagnetic radiation from the Sun (Fig. 2.1). This introduces the fourth matter of state, plasma, a gas of charged particles that dominates large volumes of the Universe. In near-Earth space, actually in most astrophysical environments, plasma consists of positive ions and negative electrons. Several species of ions can be present, such as oxygen ions and protons. Plasma is quasi-neutral. In other words the charge density of positive particles is always very close to the charge density of negative particles. If the plasma deviates from this quasi-neutrality, strong electric fields will be generated to restore it. Plasma is the most common state of matter in the visible Universe.

2.2 Characterization

Every plasma species can be characterized by its number density, n and temperature, T. In space physics temperature [2] is defined as the average kinetic

[1] The standard in space physics is 1 Re = 6371 km.

[2] It is standard in space physics to use electron volt (eV) as the unit to measure plasma temperature or any other energy quantity. The relation between temperature, T, expressed in K T[K], or in eV, T[eV] and energy, E, expressed in Joules is given by:

$$\mathrm{E[J]} = k_b \mathrm{T[K]} = e\mathrm{T[eV]}, \tag{2.1}$$

where e is the elementary charge and k_b is the Boltzmann constant. From equation 2.1 we obtain a conversion factor for temperature of 1 eV = 11600 K.

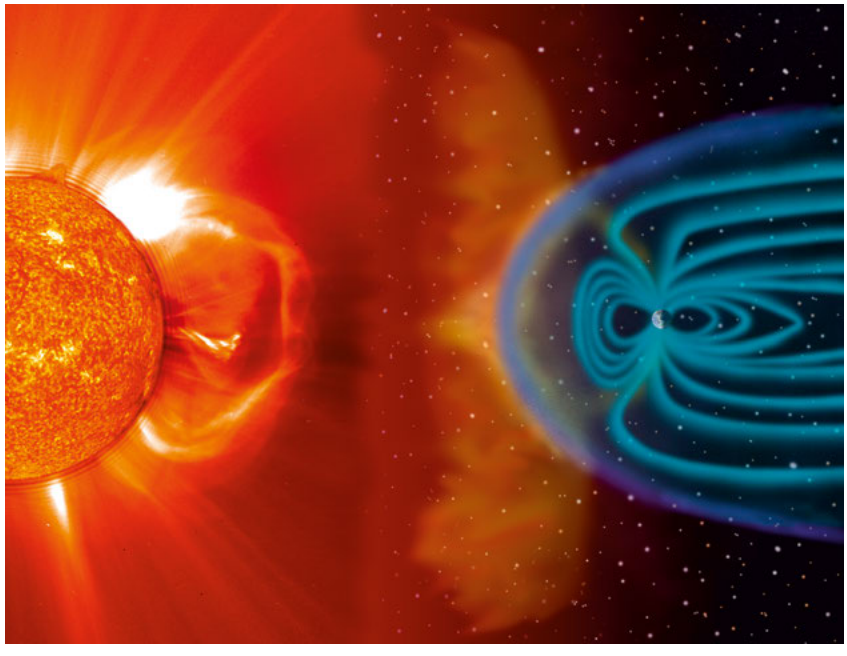

Figure 2.1. Artist rendition of the Sun and Earth relationship. Credit: NASA/Steele Hill.

energy of particles in the reference frame moving with the average particle velocity. In the outer magnetosphere plasma is collisionless and due to different physical processes heating them, different plasma species can have different temperatures.

While density and temperature of plasma species are fundamental parameters characterizing plasma, they are not the only important parameters. For example, the ratio between plasma pressure and magnetic field pressure (plasma beta β) and the magnetic field strength are important parameters controlling physical processes in the plasma. The motion of charged particles can be affected if electric fields are present in the plasma. Particle distribution functions, so called phase space densities, can have anisotropies with respect to the magnetic field. Different plasma waves can be present, there can be large-scale gradients in the plasma, etc. All this makes plasma a very interesting and complex environment to study.

2.3 Important Plasma Equations

Since plasma is made up of positive ions and negative electrons, electromagnetic interactions are important. Electromagnetic interactions are controlled

by a set of combined equations commonly referred to as Maxwell's equations:

$$\nabla \cdot \mathbf{E} = \frac{\rho}{\epsilon_0} \tag{2.2}$$

$$\nabla \cdot \mathbf{B} = 0 \tag{2.3}$$

$$\nabla \times \mathbf{E} = -\frac{\partial \mathbf{B}}{\partial t} \tag{2.4}$$

$$\nabla \times \mathbf{B} = \mu_0 \mathbf{J} + \mu_0 \epsilon_0 \frac{\partial \mathbf{E}}{\partial t} \tag{2.5}$$

where equation 2.2 is Gauss' law, equation 2.4 is Faraday's law, and equation 2.5 is Ampére's law. $\mathbf{J} = e(n_i \mathbf{u_i} - n_e \mathbf{u_e})$ is the total current density where $\mathbf{u_i}$ and $\mathbf{u_e}$ are the ion and electron bulk velocity, respectively, $\mathbf{E}$ and $\mathbf{B}$ are the electric and magnetic field, respectively. $\rho = e(n_i - n_e)$ is the total charge density, e is the elementary charge, μ_0 is the permittivity of free space, and ϵ_0 is the vacuum permittivity. Gauss' law states that $\mathbf{E}$ will diverge (converge) near positive (negative) charges and if there are no charges $\mathbf{E}$ is divergence free. Equation 2.3 states that there are no magnetic charges, in other words $\mathbf{B}$ is divergence free. Faraday's law states that a curl of $\mathbf{E}$ means there is a time varying $\mathbf{B}$ or vice versa and Ampére's law essentially says that if $\nabla \times \mathbf{B} \neq 0$, a current and/or a time varying $\mathbf{E}$ exist or vice versa. The second term on the r.h.s of Ampére's law is usually referred to as the displacement current.

If we assume that $\mathbf{J}$ is related to $\mathbf{E}$ and $\mathbf{B}$ in the plasma through Ohm's law with the conductivity, σ,

$$\mathbf{J} = \sigma(\mathbf{E} + \mathbf{v} \times \mathbf{B}), \tag{2.6}$$

and neglect the displacement current in Ampére's law (equation 2.5), then Faraday's law (equation 2.4), can be rewritten as the induction equation:

$$\frac{\partial \mathbf{B}}{\partial t} = \frac{1}{\mu_0 \sigma} \nabla^2 \mathbf{B} + \nabla \times (\mathbf{v} \times \mathbf{B}) \,. \tag{2.7}$$

The induction equation shows how $\mathbf{B}$ evolves with time, where the first term on the r.h.s. is the diffusive term and the last term is the advective term. If the advective term is the only term on the r.h.s of the induction equation then $\mathbf{B}$ can be thought of as being "carried" along with the plasma at velocity $\mathbf{v}$, the plasma is "frozen-in". Quotations are used because magnetic field lines are only a construct to simplify the visualization of the evolution of $\mathbf{B}$ and are not physically real.

2.4 Kinetic Theory

In this thesis the term kinetic study comes up. In a kinetic description of plasma, particle distribution functions, $f(\mathbf{r}, \mathbf{v}, t)$, are used (Fig. 2.2). A particle

distribution function gives the probability density of finding a particle at a point $\mathbf{r}$ with velocity $\mathbf{v}$ at the time t. Different characteristic parameters of plasma, such as pressure $\overline{\overline{\mathrm{P}}}$, $\overline{\overline{\mathrm{T}}}$, n, and the bulk flow velocity $\mathbf{u}$ can be determined by calculating different moments of a distribution function:

$$n(\mathbf{r},t) = \int_{-\infty}^{\infty} \mathrm{f}(\mathbf{r},\mathbf{v},t)d^3v, \tag{2.8}$$

$$\mathbf{u}(\mathbf{r},t) = \frac{1}{n}\int_{-\infty}^{\infty} \mathbf{v}\mathrm{f}(\mathbf{r},\mathbf{v},t)d^3v, \tag{2.9}$$

$$\overline{\overline{\mathrm{P}}}(\mathbf{r},t) = m\int_{-\infty}^{\infty} \mathrm{f}(\mathbf{r},\mathbf{v},t)(\mathbf{v}-\mathbf{u})(\mathbf{v}-\mathbf{u})d^3v, \tag{2.10}$$

$$\overline{\overline{\mathrm{T}}}(\mathbf{r},t) = \frac{\overline{\overline{\mathrm{P}}}}{nk_b}, \tag{2.11}$$

where both $\overline{\overline{\mathrm{P}}}$ and $\overline{\overline{\mathrm{T}}}$ are tensors and k_b is the Boltzmann constant. By taking the mean of the trace of the respective tensors the scalar temperatures and pressures can be determined. The scalar temperature and pressure is the one typically shown in observations plots if nothing else is specified in the figure caption.

To solve many physical problems, such as which acceleration mechanism is involved, the moments of the distribution function are not enough. Instead the full distribution function and its evolution is needed. A kinetic description of a plasma refers to the description of a distribution function's evolution. By assuming collisionless plasma, the simplest possible form of equation, the *Vlasov equation*, describing the evolution is derived:

$$\frac{\partial \mathrm{f}(\mathbf{r},\mathbf{v},t)}{\partial t} + \mathbf{v}\bullet\nabla\mathrm{f}(\mathbf{r},\mathbf{v},t) + \frac{e}{m}(\mathbf{E}+\mathbf{v}\times\mathbf{B})\bullet\frac{\partial \mathrm{f}(\mathbf{r},\mathbf{v},t)}{\partial \mathbf{v}} = 0. \tag{2.12}$$

The Vlasov equation can be interpreted as $\mathrm{f}(\mathbf{r},\mathbf{v},t)$ is constant along a particle's orbit in space (Liouville's Theorem).

2.5 Terminology

In this thesis we use words such as heating, acceleration, and energization. They are all related to the distribution function. When we use the term heating what we mean is an increase of temperature like illustrated in Fig. 2.3. Acceleration on the other hand is a more loosely defined process where only some fraction of the particles is accelerated to higher energies. Acceleration can appear as well resolved beams (Fig. 2.4a) and/or as power law tails (Fig. 2.4b) in the distribution functions. When we use the term energization what we refer to is observations of both heating and acceleration.

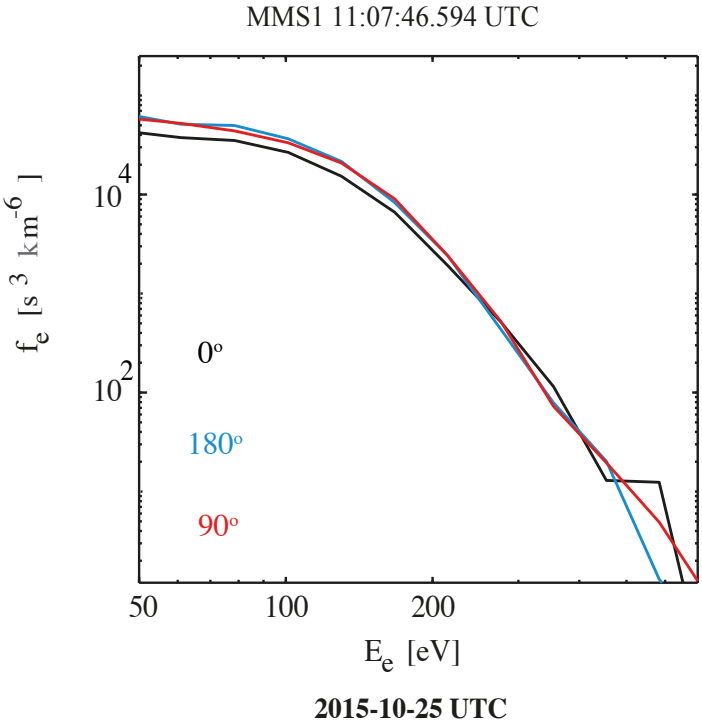

Figure 2.2. Example of an electron distribution function observed by MMS on October 25, 2015 where 0°, 180°, 90° refers to the direction parallel, antiparallel, and perpendicular to **B**, respectively. Adapted from Eriksson et al. (2016).

2.6 Kinetic Scales

Another important term in acceleration studies is kinetic scales. At large scales, a fluid description of a plasma can often accurately describe plasma processes. However, at smaller scales, the so called kinetic scales, the particle's own motion needs to be considered and usually requires a kinetic description of the plasma. Characteristic kinetic scales are inertial lengths and gyroradii. A particle's gyroradius r_g is the radius of a particle's gyration about **B**

$$r_g = \frac{m_s v_{s,\perp}}{|e|B}, \tag{2.13}$$

where s refers to the particle species and $v_\perp$ is the speed of species s perpendicular to **B**. The electron d_e and ion inertial d_i lengths scales, sometimes referred to as the electron and ion skin depths, are given by:

$$d_e = \frac{c}{\omega_{pe}}, \tag{2.14}$$

$$d_i = \frac{c}{\omega_{pi}}, \tag{2.15}$$

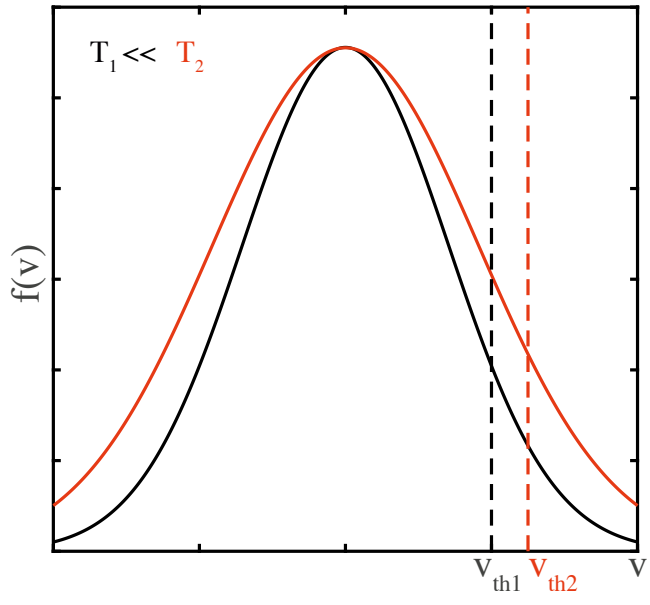

Figure 2.3. Illustration of heating assuming a maxwellian distribution, the most common theoretical particle distribution function, where the red distribution has higher temperature than the black.

where c is the speed of light, $\omega_{pe} = \sqrt{\frac{ne^2}{m_e \epsilon_0}}$ is the electron plasma frequency, and $\omega_{pi} = \sqrt{\frac{ne^2}{m_i \epsilon_0}}$ is the ion plasma frequency. Normally ion kinetic scales are significantly larger than electron kinetic scales. Thus, we can have an acceleration mechanism at kinetic scales for ions that requires a kinetic description of ions, while the electrons are still "frozen-in" to **B** and can be accurately described as a fluid. The multi-spacecraft mission MMS allows kinetic description of both ions and electrons at their kinetic scales.

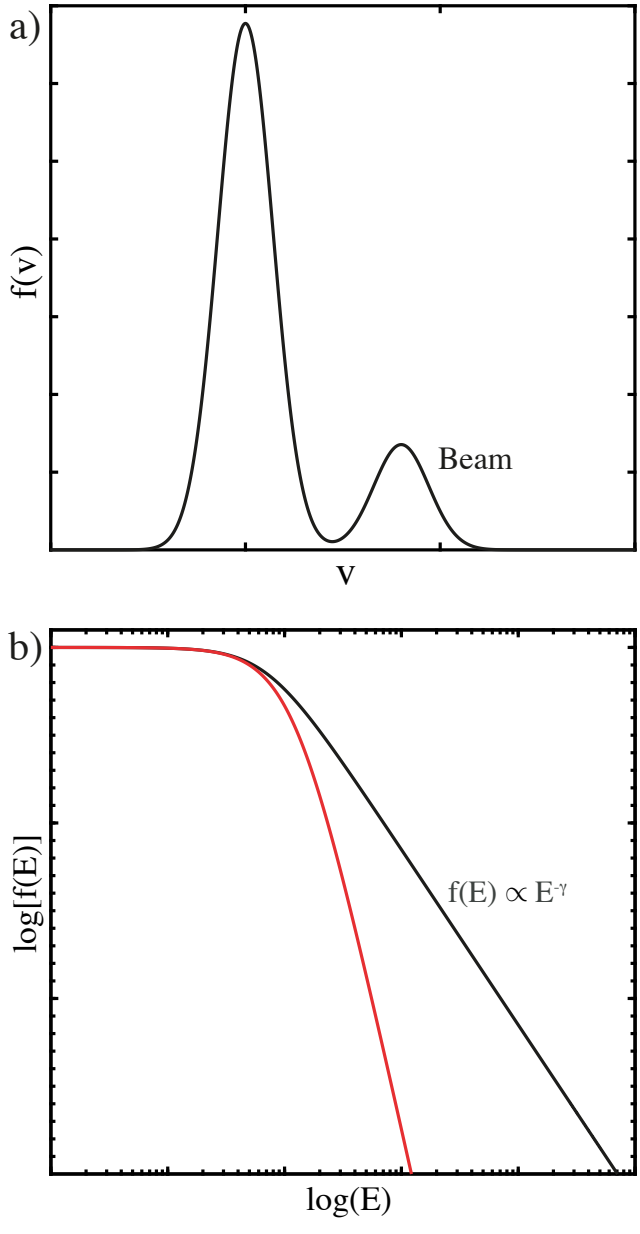

Figure 2.4. Illustration of acceleration features: a) beam and b) power-law tail (black) where the red line shows a maxwellian distribution for contrast.

3. Magnetosphere

This thesis is based on observations made in Earth's magnetosphere. Detailed information regarding Earth's magnetosphere can be found in textbooks such as Baumjohann and Treumann (1996), Kivelson and Russell (1996), and Russell et al. (2016a). This chapter gives only a brief introduction to the most basic regions that is of relevance to the articles in this thesis.

The term magnetosphere refers to a space surrounding a planet where the planet's magnetic field controls the motion of the plasma particles. The plasma in the Earth's magnetosphere consists of ions (mainly protons) and electrons originating from the ionosphere and solar wind. The boundary that separates the **I**nterplanetary **M**agnetic **F**ield (IMF) originating from the Sun and the Earth's own magnetic field (the geomagnetic field), is called the magnetopause. The geomagnetic field is what prevents almost all of the solar wind plasma from entering the magnetosphere and maybe later our atmosphere. Due to solar eruptions and solar wind velocity variations, the direction of IMF at Earth varies. Figure 3.1 shows a two-dimensional (2-D) illustration of the magnetosphere. In the figure the main components of the magnetosphere are marked: the cusps, the plasmasphere, the magnetotail with its tail lobes, the plasma sheet, the bow shock, the magnetosheath, and the magnetopause.

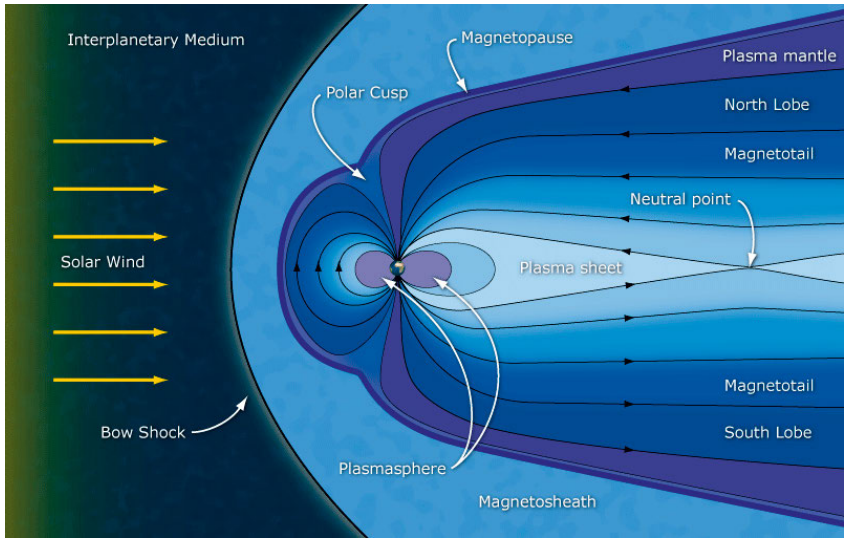

Figure 3.1. 2-D sketch of the Earth's magnetosphere. Credit: ESA/C. T. Russell.

Upstream of the magnetosphere a bow shock is formed where the supersonic solar wind is slowed down to a subsonic speed. The bow shock is typically divided into two regions, quasi-parallel and quasi-perpendicular. The names refer to the value of the angle between the bow shock normal and the IMF direction, which directly influence the behaviour of the shock itself and the plasma conditions upstream and downstream of the shock. If the angle is smaller than 45° then the bow shock is considered quasi-parallel while an angle larger than 45° indicate that the shock is quasi-perpendicular. The magnetosheath downstream of the quasi-parallel shock is one of the most turbulent plasma environments in near-Earth space (Retinò et al., 2007), where large variations in the magnetic field, plasma density, and velocity are observed. Electron acceleration and heating is very efficient here (Retinò et al., 2007; Chasapis et al., 2015). Inside the turbulent magnetosheath exist prominent features such as magnetosheath jets (yellow regions inside the magnetosheath in Fig. 3.2). Magnetosheath jets are defined as regions where the local dynamic pressure $P_{dyn} = \rho_i V_{i,x}^2$ is much larger than the dynamic pressure in the solar wind (Plaschke et al., 2013). Simulations suggest that magnetosheath jets are a possible generator of thin reconnecting current sheets and helps drive turbulence in the surrounding region (Karimabadi et al., 2014; Omidi et al., 2016). Both current sheets studied in Article II and III are located at a magnetosheath jet.

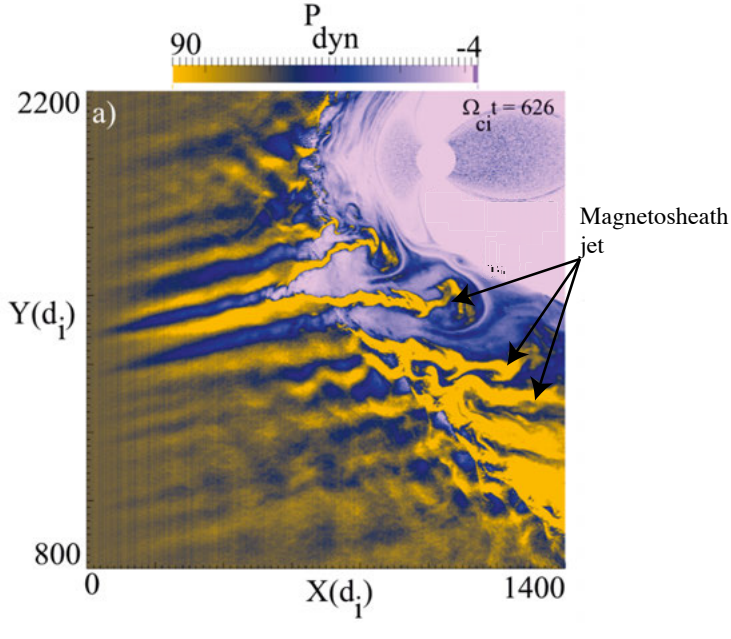

Figure 3.2. Results from a global-hybrid simulation showing dynamic pressure around the quasi-parallel bow shock. The black arrows point towards magnetosheath jets. Adapted from Karimabadi et al. (2014).

The polar cusps form at high latitudes and for southward IMF separates closed magnetic field lines on the dayside from the open field lines pulled away by the solar wind to the magnetotail. The cusps are important because they are the weak spots of the magnetosphere, the places where plasma particles from the solar wind can directly penetrate the magnetosphere along the magnetic field lines. The lobes are regions with low density and open field lines: one end is connected to the solar wind while the other is connected to the Earth.

The conditions inside and between all the regions of the magnetosphere determine how solar wind particles enter our magnetosphere. That is why it is important to study how particles are accelerated between and inside these regions. In this thesis we focus on acceleration of electrons inside the turbulent magnetosheath (Article II and III) and the magnetotail (Article IV). We also perform a statistical study of magnetic nulls, a magnetic structure believed to be important for particle acceleration, in the nightside magnetosphere (Article I).

4. Magnetic Reconnection

In most parts of the Universe, a good approximation is that the magnetic field is being “carried” along the plasma, the plasma is “frozen-in” to the magnetic field. However, magnetic reconnection (Fig. 4.1), a fundamental plasma process, occurs in some localized regions and breaks the “frozen-in” condition allowing plasma to move between different magnetic field lines (Priest and Forbes, 2000; Priest, 2003; Birn and Priest, 2007). During reconnection magnetic energy is converted into heating of the plasma and particle acceleration. Magnetic reconnection has been observed, or has been suggested to be present, in the chromosphere (e.g., Hong et al., 2016), the solar wind (e.g., Gosling et al., 2005), Earth’s magnetosphere (e.g., Hasegawa et al., 2007; Nagai, 2006; Retinò et al., 2007; Xiao et al., 2007; Phan et al., 2007), galaxies (e.g., Wezgowieca et al., 2016), comet tails (e.g., Jovanovic et al., 2005), and even on other planets such as Saturn (e.g., Arridge et al., 2016). However, there are still many unanswered questions related to the physics of magnetic reconnection, in particularly, which mechanisms are important for accelerating electrons at sub-ion scales.

For reconnection to occur a sharp change in the magnetic field, a so called shear, is needed which by its very definition implies the existence of a region of strong current (Ampére’s law). If the current region has a planar geometry, it is usually referred to as a current sheet. An electric field is also required to break the “frozen-in” condition. As reconnection proceeds, plasma jets are formed due to the magnetic tension force from the newly reconnected field lines (from the "straightening" of the field lines), strong currents are generated, plasma is heated, and many other processes take place. How exactly the reconnection electric field is generated is an open question. The resistive term in the resistive Ohm’s law (equation 2.6) is generally not large enough to break the “frozen-in” condition in collisionless space plasmas (Birn and Priest, 2007). Instead, it can be anomalous resistivity due to plasma waves or non-gyrotropic electron distributions that allow the generation of the reconnection electric field. There are also processes that can suppress reconnection. Velocity shears, for example, can suppress reconnection (Cowley and Owen, 1989; Doss et al., 2015; Doss et al., 2016). Figure 4.2 illustrates the concept, where $V_A = B/\sqrt{\mu_0 m_i n}$ is the Alfvén speed, a typical ion outflow jet speed. If the velocity shear V_{shear} is larger than the ion outflow speed generated by the magnetic tension force, reconnection will be suppressed. Understanding how reconnection work is a major goal of space physics. The multi-spacecraft mission MMS is fully dedicated to this problem.

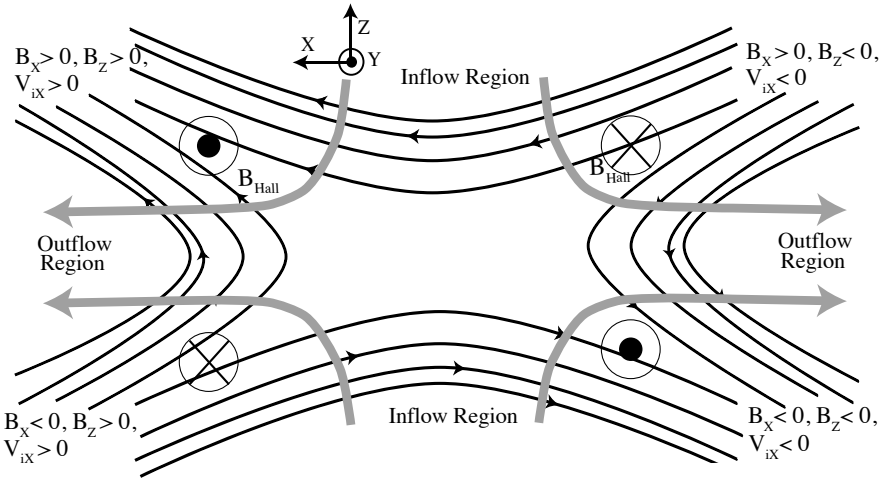

Figure 4.1. Illustration of the 2-D reconnection diffusion region, where the "frozen-in" condition breaks down. The magnetic field is given by the black arrowed lines. The spacing between the lines indicate the magnetic field strength, where larger spacing means lower field strength. The large grey arrows gives the average ion flow through the diffusion region. The out-of-plane magnetic field is the so called Hall magnetic field generated by the decoupling of ions and electrons from the magnetic field at different scales.

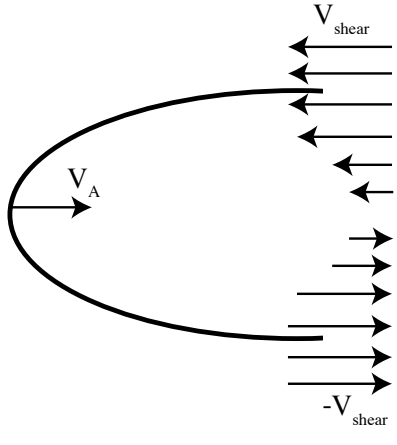

Figure 4.2. Illustration of the relationship between reconnection and velocity shear, where V_A is a typical ion outflow speed and V_{shear} is the velocity shear.

5. Magnetic Nulls

Magnetic nulls, regions of vanishing magnetic field, can be important sites of energy release and particle acceleration (Priest and Forbes, 2000; Birn and Priest, 2007, and references therein). Nulls, both as pairs and single occurrences, have been observed in reconnection current sheets in the Earth's magnetotail (Xiao et al., 2006; Xiao et al., 2007; He et al., 2008; Deng et al., 2009; Wendel and Adrian, 2013). Solar events like brightening of a flare (Chen et al., 2016), solar jets (Zeng et al., 2016), and CME's (Lynch et al., 2008) are also believed to be connected with reconnection at three-dimensional (3-D) nulls. Magnetic nulls have also indirectly been found in abundance in the corona (Freed et al., 2015). The reason why magnetic nulls are believed to be possible sites of particle acceleration is because near them plasma particles become unmagnetized, due to the low magnitude of the magnetic field strength, and can directly propagate along an electric field. A strong electric field is expected from reconnection theory so particles near reconnecting nulls can theoretically be accelerated to high energies by traveling along the electric field. Magnetic nulls are the topic of Article I.

The magnetic topology around a magnetic null can be different and it determines what kind of plasma processes, such as reconnection, that can occur at the null (Birn and Priest, 2007). The magnetic topology of a null can be characterized by its type based on the direction of the magnetic field in the null's *skeleton* (Cowley, 1973; Lau and Finn, 1990). The skeleton is separated into two structures (Fig. 5.1): *the fan plane* where the magnetic field is either directed in or out of the null, and *the spine* where the magnetic field is either directed in or out of the null. The fan is a plane and acts as a "surface separatrix" separating two topologically unique regions, while the spine is a tube. The skeleton can be found and re-created by assuming linear magnetic field $\mathbf{B}$ around the null using a first order Taylor expansion:

$$\mathbf{B}(\mathbf{r}) = \nabla\mathbf{B} \bullet (\mathbf{r} - \mathbf{r}_n)\,, \tag{5.1}$$

where $\mathbf{r}$ is the location in space, $\mathbf{r}_n$ is the null position, and $\nabla\mathbf{B}$ is the gradient of the magnetic field that requires at least four spacecrafts to determine. Thus, only multi-spacecraft missions like Cluster and MMS can determine a null's type.

In general, the eigenvalues, $\lambda_1, \lambda_2, \lambda_3$, and corresponding eigenvectors of $\nabla\mathbf{B}$ (no matter which coordinate system it is in), defines the spine and fan of a 3-D null. Depending on the eigenvalues the nulls are either classified as A, B,

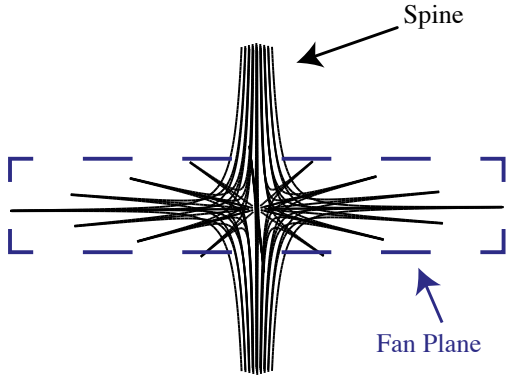

Figure 5.1. Illustration of the skeleton of a 3-D magnetic null.

As, or Bs type (Cowley, 1973; Greene, 1988; Lau and Finn, 1990) (Fig. 5.2). From equation 2.3 (no magnetic charges) we know that the eigenvalues must satisfy the condition $\lambda_1 + \lambda_2 + \lambda_3 = 0$. Thus, the fan plane is spanned by the two eigenvectors corresponding to the eigenvalues whose real parts have the same sign. If the eigenvalues in the fan are complex the magnetic field will spiral about the null point, hence the name spiral nulls (As/Bs). The other two types (A or B) are usually referred to as radial nulls. The direction of the field along the spine is given by the sign of $\det(\nabla \mathbf{B}) = \lambda_1 \cdot \lambda_2 \cdot \lambda_3$ (Lau and Finn, 1990). A/As nulls (referred to as A kind in Article I) have a positive $\det(\nabla \mathbf{B})$ value, which means that $\mathbf{B}$ diverge away from the null point along the spine and converge toward the null point in the fan plane. The other types of nulls, Bs/B (referred to as B kind in Article I), have the reversed direction of $\mathbf{B}$ with a negative value of $\det(\nabla \mathbf{B})$. In Article I we use the null's *skeleton* to create a null identification reliability method (see section 7.2) and show how localized magnetic field fluctuations affect the null type identification.

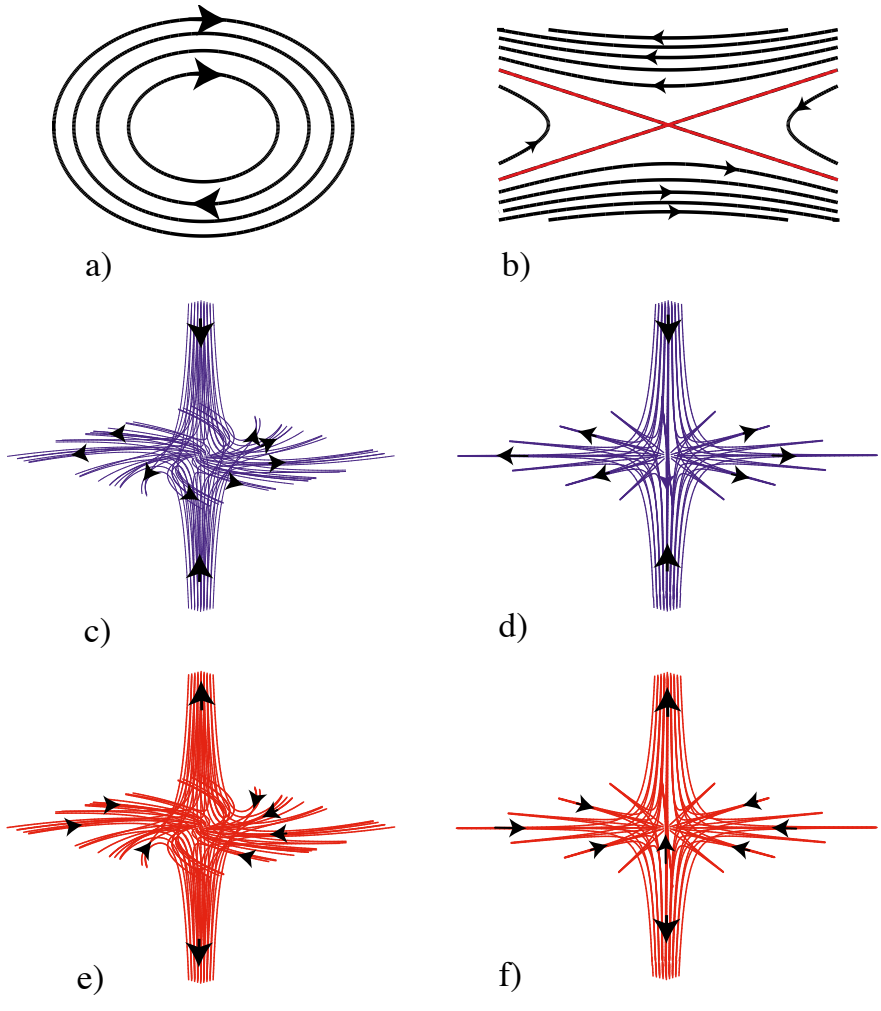

Figure 5.2. Illustration of different null types. 2-D types: a) O-line , b) X-line. 3-D types: c) Bs, d) B, e) As, f) A. The black arrows indicate the direction of the magnetic field.

6. Spacecraft Missions and Instruments

This chapter contains a brief introduction to Cluster and MMS. For each spacecraft we have included a short section explaining the basic operation and some of the limitations of the instruments used in this thesis.

6.1 Cluster

Cluster (Fig. 6.1) is a four spacecraft mission from the **E**uropean **S**pace **A**gency (ESA). The spacecraft were launched a month apart into a polar orbit on the 16 July, 2000 and 9 August, 2000 with an apogee and perigee of about 19 and 4 Re, respectively (Escoubet et al., 2001). Cluster is still an active mission and has now been in space for 18 years. The possibility of changing the separation between the spacecraft and the evolution of the orbit makes it possible for Cluster to investigate different regions of the Earth's plasma environment. The main goal of Cluster is to study 3-D plasma structures such as reconnection. To achieve 3-D measurements and the ability to distinguish spatial and temporal changes, Cluster has four spacecraft flying in a tetrahedron configuration. Each spacecraft carry an identical set of 11 instruments, which includes fields instruments, that measures the electric and magnetic field, as well as particle instruments measuring negatively charged electrons and positively charged ions. Details on different kinds of discoveries made with Cluster can be found e.g., in Escoubet et al. (2013).

6.1.1 Fluxgate Magnetometer (FGM)

A **F**lux**G**ate **M**agnetometer (FGM) measures the slowly varying magnetic field. Most modern fluxgates magnetometers have a tri-axial arrangement of three sensors so three components of the magnetic field can be measured. A fluxgate sensor consists of a magnetic core that for each half period is driven to saturation by an alternating current. If there is no external magnetic field then the output from doing this is symmetrical. If, however, an external magnetic field is present then the saturation occurs faster and the periodic variation in the magnetic flux becomes asymmetrical. The degree of the asymmetry is proportional to the external magnetic field. However, a spacecraft will also generate its own magnetic and electric field. Therefore, the magnetometers are placed on solid booms away from the spacecraft where the spacecraft's own fields affect the measurements the least.

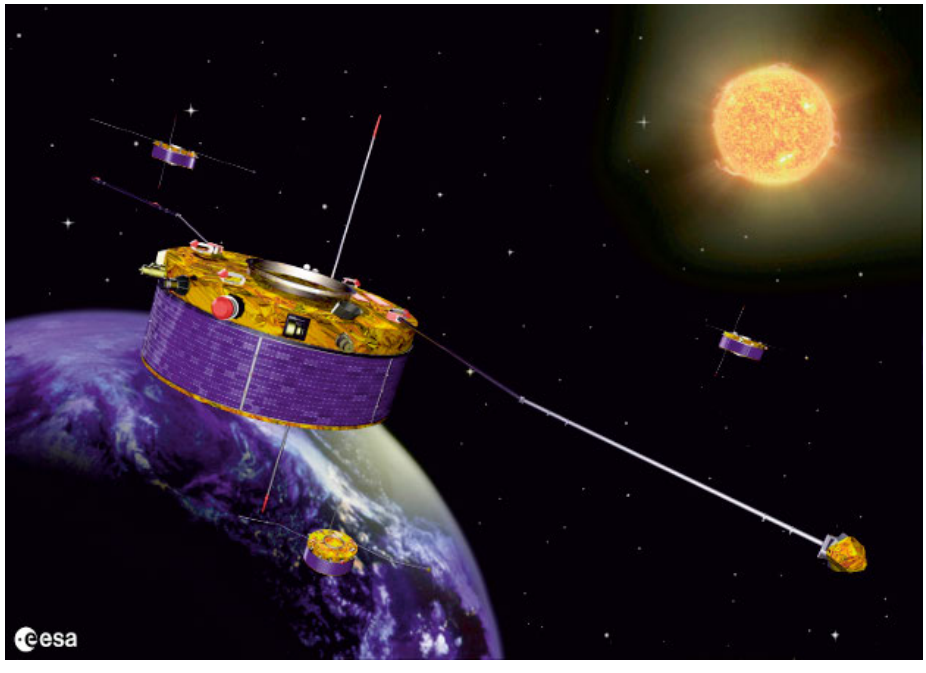

Figure 6.1. Artist rendition of the Cluster mission. Credit: ESA.

Each Cluster spacecraft carries an identical FGM instrument which consists of two triaxial fluxgate magnetometers and accompanying electronics. Each spacecraft has a 5.2 m long radial solid boom that was extended after launch; one of the magnetometers is placed at the end of the 5.2 m boom while the second magnetometer is placed 3.7 m outward on the same boom. Due to the operational design of the instrument the most common errors that are adjusted for during ground calibration is offsets due to the electronics and offsets due to the spacecrafts own magnetic field. For Cluster the accuracy for FGM when the magnetic field magnitude is less than 200 nT, as was the case in Article I, is 0.1 – 0.2 nT (Gloag et al., 2010). This means that care should be taken when evaluating structures of low magnetic field magnitude such as magnetic nulls, the topic of Article I. In Article I the magnetic field is measured at 67.3 Hz (15 ms).

6.2 Magnetospheric MultiScale (MMS)

MMS is a multi-spacecraft mission from **N**ational **A**eronautics and **S**pace **A**dministration (NASA) that was launched on March 12, 2015 (Burch et al., 2016). Like Cluster, MMS is a four spacecraft mission that is flying in a tetrahedron configuration (Fig. 6.2). However, MMS's orbit is different from

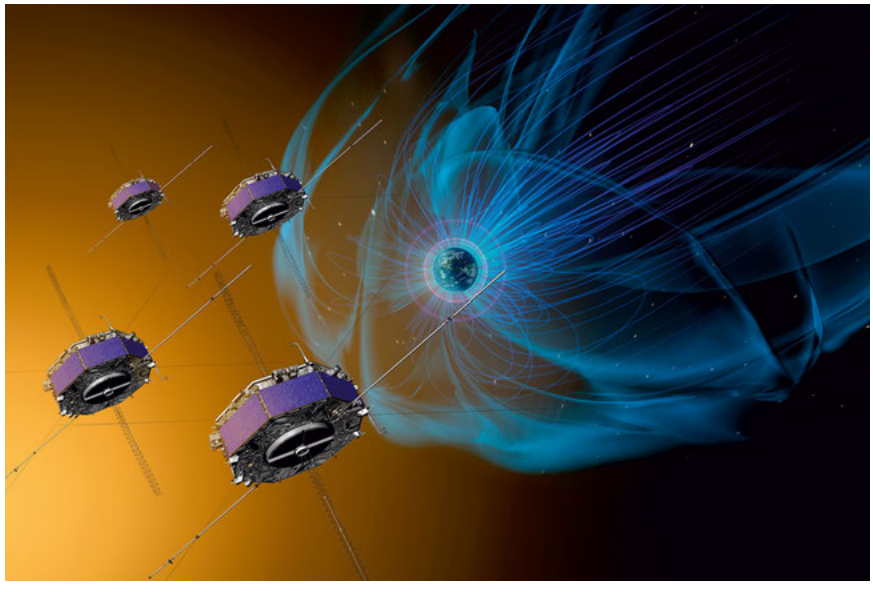

Figure 6.2. Artist rendition of the MMS mission. Credit: NASA.

Cluster's. The orbit is highly eccentric and equatorial. MMS has three main goals and they are to: (1) determine the role of turbulent dissipation and electron inertial effects in the tiny region in reconnection where the electrons decouple from the plasma, commonly referred to as the **E**lectron **D**iffusion **R**egion (EDR) predicted by 2-D reconnection theory, (2) determine what role the ion inertial effects have on reconnection, and (3) determine the parameters that control the reconnection rate and what that rate is. To do that MMS spacecraft are flying in a much tighter spacecraft configuration compared to Cluster, about 7-20 km separation for the dayside phases and 20-160 km for the nightside phases. In the beginning of the mission the dayside phases had a larger separation of 60-100 km. The orbit of the spacecraft is optimized so that the spacecraft gather as much data as possible near expected reconnection sites (Burch et al., 2016; Fuselier et al., 2016). Thus, the apogee started at the dayside phases at 12 Re, to cover magnetopause reconnection, and was later increased to 25 Re for the nightside phases, to cover magnetotail reconnection (Fuselier et al., 2016). Each spacecraft carry an identical set-up of 16 instruments, including particle detectors, electric, and magnetic field instruments (Fig. 6.3).

Because the EDR is predicted to be incredibly small and reconnection regions are generally very fast moving, the spacecraft instruments and their orbit were designed in such a way that the spacecraft could have a high enough sampling rate near the expected regions of reconnection. For example, an EDR moving with 50 km s^{-1} with a typical width of 5 km would be crossed by a spacecraft in only 0.1 s. Thus, the time resolution of e.g., the particle

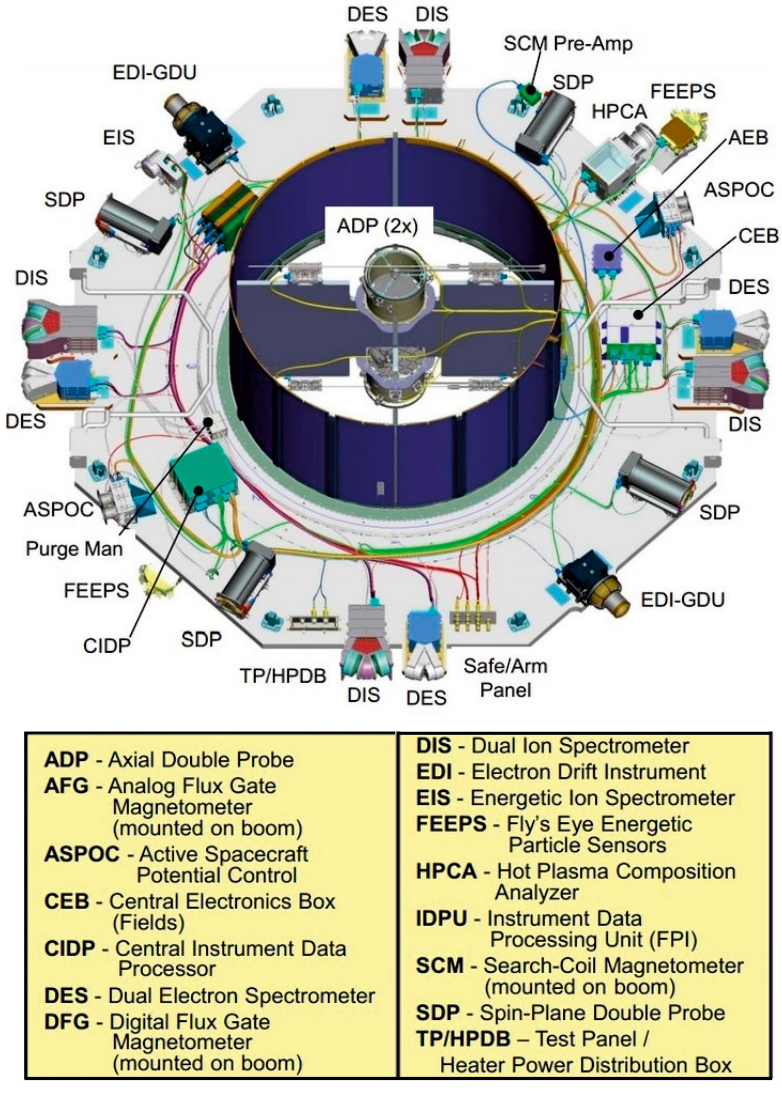

Figure 6.3. MMS instrument sketch showing the location of all instruments, where the explanation for each instrument acronym can be found in the yellow box. Credit: NASA.

instrument **F**ast **P**lasma **I**nvestigation (FPI) (Pollock et al., 2016) of 0.03 s at which the electron distribution functions are measured allows us to obtain at least three measurements of the electron distribution function during the crossing. Similarly, using the length scales of the ion diffusion region the time resolution for the ions of 0.15 s of FPI allows up to 30 measurements inside the ion diffusion region. Thus, both electron and ion distribution functions can be well resolved within their respective diffusion regions. Of course, if

the studied region is sub-ion scale like in Article III the ion resolution is not sufficient to resolve localized ion structures inside it, if there are any. In articles II-IV we use particle and field measurements from FPI (Pollock et al., 2016), FGM (Russell et al., 2016b), **S**earch-**C**oil **M**agnetometer (SCM) (Le Contel et al., 2016), and **E**lectric Field **D**ouble **P**robes (EDP) (Lindqvist et al., 2016; Ergun et al., 2016) onboard the MMS spacecraft.

6.2.1 Fast Plasma Investigation (FPI)

FPI measures ions and electrons distributions between 10 eV to 30 keV. The FPI instrument includes eight sensors per species (ion/electron) around the spacecraft body (DES and DIS in Fig. 6.3). This allows measurements in all directions independent of the spacecraft spin, unlike the Cluster mission where the 3-D particle distributions are constructed using data from a full spin of the spacecraft, a so called spin period (Fazakerley et al., 2010; Dandouras et al., 2010). Each sensor allows their respective particle to enter through an aperture. After entering particles move through an electrostatic analyzer which only lets through particles in a narrow energy band around the energy defined by the applied electrostatic potential. The passing particles will reach the sensor's detector and be counted. These counts are then translated into a 3-D distribution function between 10 eV and 30 keV and is normally given every 30 ms for electrons and 150 ms for ions. An electron distribution function with a time resolution of 7.5 ms can be requested from FPI (Rager et al., 2018). With such high sampling rates only about 20 min of burst data per day can be downloaded through the **D**eep **S**pace **N**etwork (DSN) and the memory on-board each spacecraft can only handle 3 days worth of data. Therefore, a scientist, the so called **S**cientist-**I**n-**T**he-**L**oop (SITL), is in charge of selecting which time intervals should be downloaded in burst mode according to a predetermined ranking system. The rest of the data is averaged down to a fast-survey rate where the time resolution of the full distribution is 4.5 s, which is comparable to previous missions such as Cluster (4s resolution) (Fazakerley et al., 2010; Dandouras et al., 2010).

Several things can affect the measurements of FPI. Two examples are background contamination and limited angular coverage in the 7.5 ms electron data. The main background contamination for electrons comes from photoelectrons, electrons that are knocked out from a spacecraft surface due to solar **U**ltra-**V**iolet (UV) photons with energy above the electron binding energy. The effect of the photoelectrons can be minimized by removing all electron data below the spacecraft potential. FPI gives a full 3-D distribution function every 30 ms, however, in cases where for example sub-ion scale structures are investigated, like in Article III, sometimes a higher time resolution of electron data is desirable. The higher time resolution distribution function contains one fourth of the full distribution function, having full coverage in polar angle,

energy, and reduced coverage in the spacecraft's azimuthal angle. Since the data has a limited angular coverage localized electron features such as beams can be missed if they arrive in the wrong angle in the spin plane.

6.2.2 Fluxgate Magnetometer (FGM)

The slowly varying magnetic field is measured by two triaxial FGMs, called the **A**nalog **F**lux**G**ate (AFG) and **D**igital **F**lux**G**ate (DFG), each with different electronic designs. Each is mounted on the end of two 5 m solid booms with connecting electronics. They work in the same manner as the ones on Cluster (see 6.1.1). FGM samples the magnetic field every 7.8 ms (128 Hz) with an accuracy of 0.1 nT for every 10 ms (Torbert et al., 2016).

6.2.3 Search-Coil Magnetometer (SCM)

The SCM (Le Contel et al., 2016) is a tri-axial search-coil magnetometer that measures fluctuations in three magnetic field components from 1 Hz to 6 kHz. It is mounted 4 m outward on the same boom as AFG is mounted. The resolution of SCM is 0.15 pT at 1kHz. The SCM measures magnetic field fluctuations using Faraday's law which states that in a coil with X number of turns the voltage is equal to the change in magnetic flux times X. In other words, the fluctuating field can be derived from the measured voltage. The SCM is used in Article II-III to study waves. In Article III we also use combined magnetic field data from FGM and the SCM due to the sub-ion scale of the studied current sheet.

6.2.4 Electric Field Double Probes (EDP)

An electric field is vital for electron acceleration. The electric field is measured in all three directions by EDP. This is achieved by having four 60 m long wire booms with a spherical probe at each end in the spin-plane, the plane perpendicular to the spacecraft's spin-axis, and two tube sensors on two 12.67 m solid booms along the spin-axis. The booms along the spin-axis are of different size and construction than the spin-axis booms, since the spin axis booms cannot use the centrifugal force from the spacecraft's spin to deploy. The electric field is sampled every 1 ms (128 Hz) with an accuracy better than 1 mV m^{-1} (Torbert et al., 2016). The electric field is determined by measuring the potential difference between opposing probe pairs and dividing it with the effective separation between the probes.

The measured electric field does not always reflect the ambient plasma's electric field. Several things can affect the electric field measurements. Two examples are: the photoelectron cloud and ion wake. The photoelectron cloud surrounding the spacecraft and electric field booms consists of photoelectrons

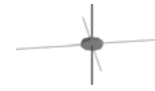

emitted from the spacecraft body, booms, and probes due to the UV radiation from the Sun. There is always more photoelectrons emitted from the sunward side of the spacecraft than the nightward side, which gives an asymmetry in the photoelectron cloud. This asymmetry can create a sunward electric field. However, this effect is decreased by the use of negatively charged guards close to the probes. An ion wake refers to the ion void that forms behind a spacecraft in a fast, cold plasma (the kinetic energy of the plasma ions is larger than their thermal energy). The wake occurs because the spacecraft becomes an obstacle for the flowing ions, and since their thermal speed is much lower than the flow, the void will not be immediately filled. If the kinetic energy of ions is also lower than the spacecraft's potential energy (tenuous plasma), then the ions will not reach the spacecraft resulting in an even larger wake region. If the electrons flow is also slow and warm (electrons thermal energy is larger than their kinetic energy), the wake void will be filled with electrons giving it a net negative potential. If one of the spacecraft probes is in the wake, the measured electric field will show a broad peak.

7. Data Analysis Methods

In this chapter we summarize the most important methods used in the thesis. The magnetic null location and the magnetic null identification reliability methods are utilized in Article I, where the identification reliability method is created by us. Timing and Minimum Variance Analysis methods are used in Article II and III. The phase speed estimates using interferometry and Liouville mapping are used in Article III and the method for estimating the power density (the energy given to electrons) of three fundamental acceleration mechanisms is used in Article IV.

7.1 Magnetic Null Location

There are several ways to identify the location of magnetic nulls in spacecraft data. One way is to cross it directly with a spacecraft. However, this is very rare. Instead four spacecraft measurements are used to suggest the presence of a null within a volume made up by the spacecraft. In Article I we use the two available multi-spacecraft methods to locate magnetic nulls using FGM magnetic field data from Cluster. In this section we briefly explain them.

7.1.1 Poincaré Index

Poincaré **I**ndex (PI) is the most commonly used location method in space observations. It calculates the topology degree using a bisection method (Greene, 1992). The method tests to see if there is a magnetic null enclosed in a volume in configuration space (x,y,z) by mapping the magnetic field values, at each time step, from the configuration space into the magnetic field space (B_x, B_y, B_z) (Fig. 7.1). If PI = ±1, the tetrahedron encloses an odd number of magnetic nulls, while PI = 0 means that an even number of null points is enclosed. It is usually assumed that the spacecraft tetrahedron is sufficiently small so that PI = 0 indicate that no magnetic null is enclosed, and PI = ±1 indicate that only a single magnetic null is enclosed.

7.1.2 Linear Interpolation

The linear interpolation method, also referred to as the **T**aylor **E**xpansion (TE) method (Greene, 1992; Fu et al., 2015; Fu et al., 2016), is based on the

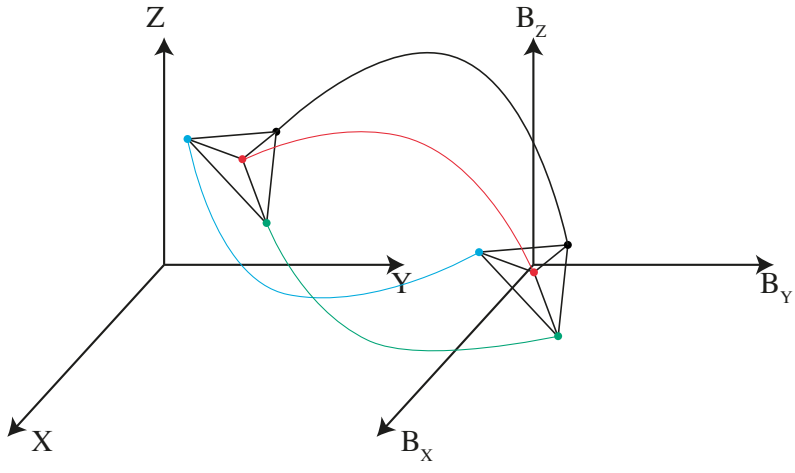

Figure 7.1. Sketch of the concept of the Poincaré index method. The different color lines represents the measurements taken by the different spacecraft.

Taylor equation (equation 5.1) used for re-creating a null's skeleton. By using positional and magnetic field measurements from four spacecraft, the position of a null can be determined by taking the inverse of equation 5.1. To use the method the gradient of the magnetic field, $\nabla\mathbf{B}$ is needed. The gradient is derived from the four spacecraft measurements by assuming the magnetic field changes linearly in space (Chanteur, 1998). Thus, the gradient is assumed to be constant in space inside the spacecraft tetrahedron. Equation 5.1 will always give a null location. How accurate that location is depends on how accurate the linearity assumption is. Extrapolations over large distances (large $\mathbf{r}-\mathbf{r}_n$) is more likely to violate the linearity assumption. Thus, in Article I the position of a magnetic null is only considered reliable if it is located inside a box volume defined by the spacecraft positions. The edges of the box in each direction (x,y,z) are given by the maximum and minimum position of the spacecraft (Fig 7.2), where the separation between all four spacecraft is required to be smaller than d_i. The separation requirement is only fulfilled in the magnetotail between July 2003 and January 2004 for Cluster.

7.2 Magnetic Null Identification Reliability

Spacecraft measurements usually suffer from problems such as instrument noise, calibration issues etc. It is therefore important to have a method for estimating what effect small magnetic field fluctuations will have on the accuracy of the type identification of magnetic nulls, since it relies on the assumption of magnetic field linearity. Furthermore, the magnetic field topology, which determines what plasma processes occur at the null, is described by a null's

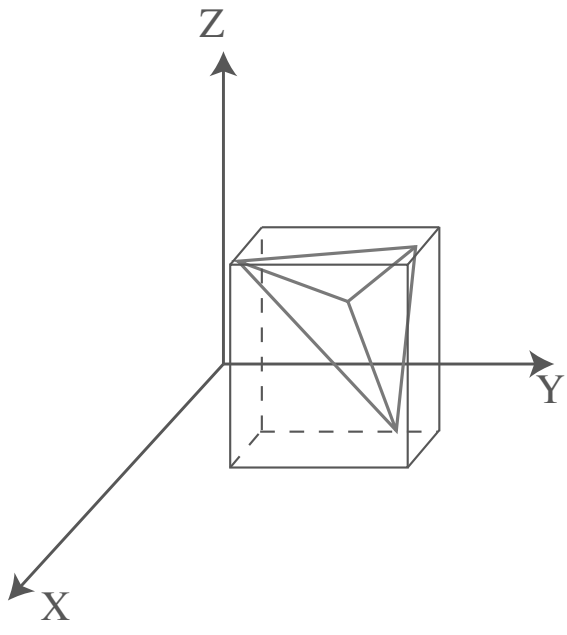

Figure 7.2. Illustration of the volume used in Article I to determine which magnetic nulls are valid.

type. When using Cluster and MMS spacecraft data the largest magnetic field disturbances originate from local plasma processes (e.g., waves or localized structures on spatial scales smaller than the spacecraft separation), but can also be due to instrumental errors. In Article I, we present our method of estimating how reliable the type identification is. In this section we give a brief summary of the method.

To create the method we used Parnell et al. (1996) method of rotating $\nabla \mathbf{B}$ into the null's coordinate system to get the parameters that defines the null's topology:

$$\nabla \mathbf{B}_{null} = s\mu_0 \begin{pmatrix} 1 & \frac{1}{2}(q - j_\parallel) & 0 \\ \frac{1}{2}(q + j_\parallel) & p & 0 \\ 0 & j_\perp & -(p+1) \end{pmatrix}, \tag{7.1}$$

where s is a scaling parameter with unit [nT km^{-1}] to make the other parameters unitless. A magnetic null is a spiral type (As/Bs) when $j_\parallel > j_{th}$ where $j_{th} = \sqrt{(p-1)^2 + q^2}$ is a threshold current derived by Parnell et al. (1996). p and q describe the potential (current free) part of magnetic field and $j_\perp$,$j_\parallel$ are the currents perpendicular and parallel to the spine of the magnetic null, respectively. The basic concept of the method is to compare theoretical minimum disturbances capable of altering the type of the null with typical magnetic fluctuations observed in the data.

There are two ways a magnetic null type can change: it can either shift between A kind or B kind, or from/to a spiral type. Using Ampéres law, the theoretical minimum disturbance required to alter a null type to/from a spiral type is

$$\delta B_1 = \mu_0 s L (j_{\parallel} - j_{th}), \tag{7.2}$$

where L is the characteristic separation between the spacecraft. Using the fact that the sign of $\det(\nabla \mathbf{B})$ determines whether the magnetic null is of A kind or B kind, the theoretical minimum disturbance required to alter a null type between A kind and B kind is

$$\delta B_2 = \min \left(|\mathbf{B}_{ij} \bullet (\mathbf{B}_{ik} \times \mathbf{B}_{il})| / |(\mathbf{B}_{ik} \times \mathbf{B}_{il})| \right), \tag{7.3}$$

where δB_2 can also be interpreted as the minimum of the inverse of a reciprocal magnetic field vector, i, j, k, l are arbitrary permutations of the four spacecraft $(1, 2, 3, 4)$, and $\mathbf{B}_{ij} = \mathbf{B}_j - \mathbf{B}_i$. Examples of how this method works can be found in Article I.

7.3 Minimum Variance Analysis

To compare observations with theories and/or simulations we first need to move the observations into the studied structure's local coordinate system. This is often done using **M**inimum **V**ariance **A**nalysis (MVA) (Sonnerup and Scheible, 1998). MVA is a single-spacecraft analytic method that makes it possible to obtain the normal direction of a structure $\hat{\mathbf{n}}$. It utilizes the assumption that the structure is one dimensional (i.e. $\frac{\partial}{\partial x} = 0, \frac{\partial}{\partial y} = 0$) and that it is stationary ($\frac{\partial}{\partial t} = 0$ in the current sheet's reference frame) when the spacecraft crosses the structure. If a spacecraft passes through a one dimensional structure, then the normal component will be constant. Thus, equation 2.3 (no magnetic charges) can be simplified to

$$\nabla \bullet \mathbf{B} = \frac{\partial B_z}{\partial z} = 0, \tag{7.4}$$

where z is the normal direction of the current sheet. $\hat{\mathbf{n}}$ is then determined by minimizing

$$\eta^2 = \frac{1}{N} \sum_{i=1}^{N} |(\mathbf{B}_{\mathrm{i}} - \langle \mathbf{B} \rangle) \bullet \hat{\mathbf{n}}|^2, \tag{7.5}$$

where $\langle \mathbf{B} \rangle = \frac{1}{N} \sum_{i=1}^{N} \mathbf{B}_{\mathrm{i}}$ and N is the number of data points in the time interval chosen to do the MVA over. After some mathematical arrangement the solution to equation 7.5 is reduced to an eigenvalue problem where three eigenvalues and their respective eigenvectors are determined. To avoid confusion with other coordinate systems the designations for the eigenvectors from MVA is

usually given by LMN. The direction of maximum, intermediate, and minimum variation is given by L, M, N, respectively. To determine the accuracy of the normal direction, one usually looks at the ratio between the M and N eigenvalues (λ_M/λ_N). The rule of thumb in space physics is that if this ratio is larger than 10 then the direction is well-defined. As an example Fig. 7.3 shows the results from the MVA of the current sheet in Article III. Note that the vectors antiparallel to the given eigenvectors from MVA are also a valid MVA coordinate system. To determine the propagation of a structure in N we need to use additional methods, such as the timing method.

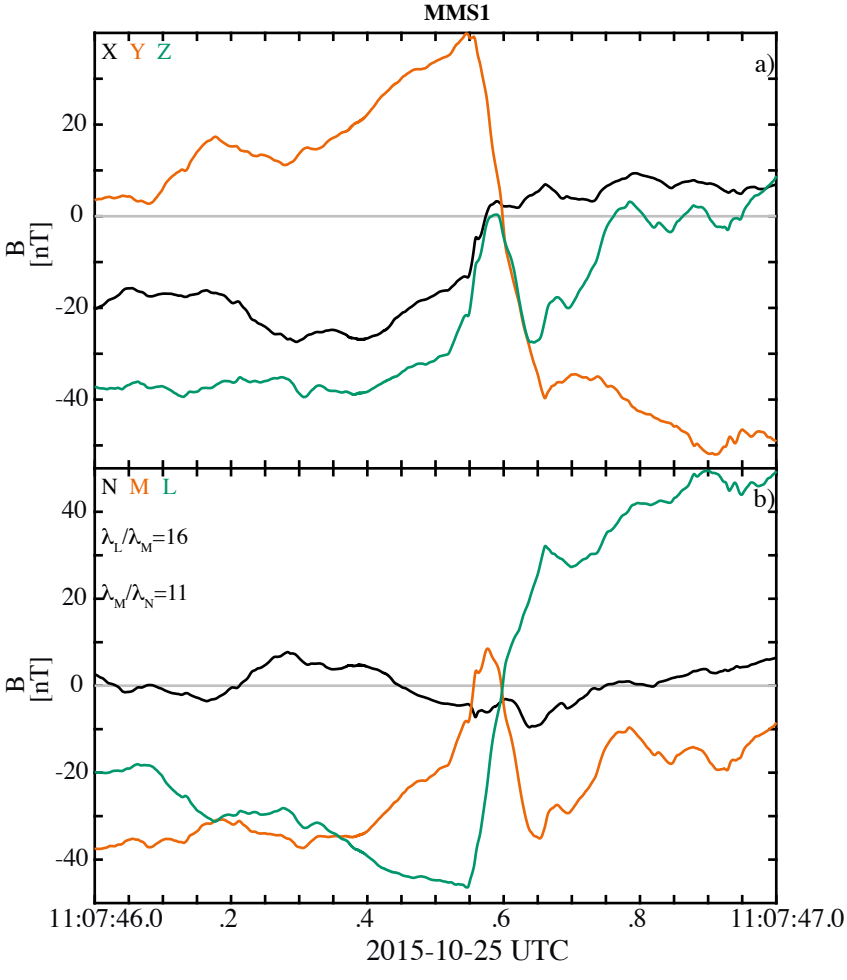

Figure 7.3. Magnetic field data from MMS1 for 1s around the current sheet studied in Article III (Eriksson et al., 2018) where a) is the magnetic field in GSE coordinates and b) is the magnetic field in LMN coordinates derived using MVA. The ratios of the different eigenvalues are given in the top left corner in panel b.

7.4 Timing

In many cases it is useful to know the normal velocity of a planar structure. If more than one spacecraft observe e.g., a wave, timing the observation of the wave between the spacecraft can help determine the wave's phase velocity. The phase velocity of a wave is important when determining if some electrons are accelerated by wave-particle interactions (see chapter 8). Timing is a common multi-spacecraft method that determines the normal velocity of a structure. Like the MVA method it relies on the assumption that the structure is one dimensional and is stationary in the structure's reference frame. The normal direction $\hat{\mathbf{n}}$ and speed V_n of the structure is calculated from the spacecraft's positions and times when they pass through the structure (Schwartz, 1998):

$$\mathbf{dS}_{\mathrm{i,j}} \bullet \frac{1}{V_n}\hat{\mathbf{n}} = dt_{i,j}, \tag{7.6}$$

where $\mathbf{dS}_{i,j} = \mathbf{r}_j - \mathbf{r}_i$ and $dt_{i,j} = t_j - t_i$ is the relative position and time difference between spacecraft i and j. V_n is commonly used to determine the thickness of a structure in N direction. This is done by multiplying the time it takes to cross the structure with the normal speed. Figure 7.5 shows the timing results for the current sheet in Article III. In panel b) we see that the time-shifted data of all four spacecraft matches up pretty well for the current sheet suggesting that the result of the timing method is reliable near the center of the current sheet.

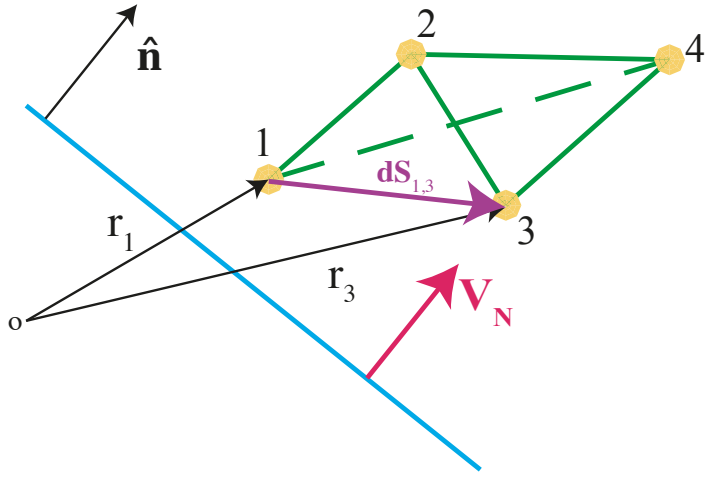

Figure 7.4. Illustration of the timing method.

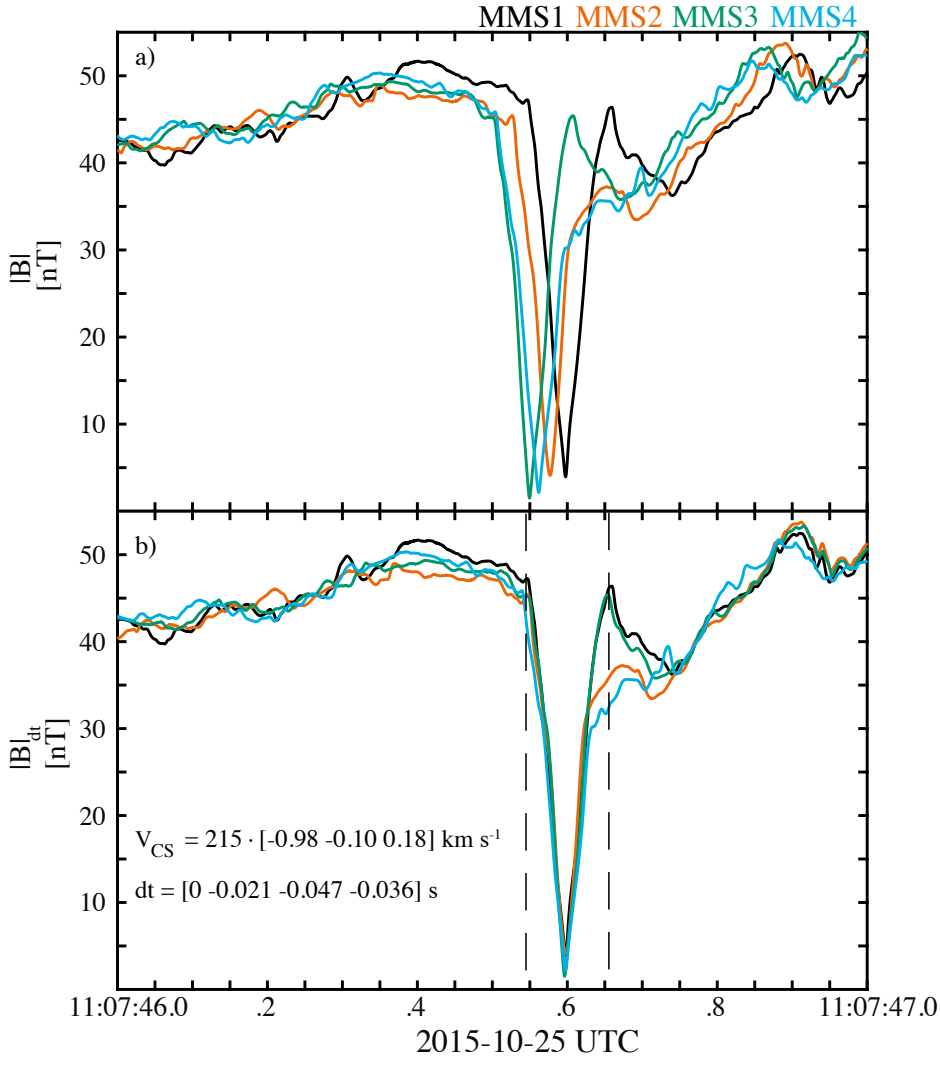

Figure 7.5. Magnetic field magnitude from all four MMS spacecraft. a) as observed, b) timeshifted data based on the timing result given in the panel, where the dotted line indicates the current sheet crossing.

7.5 Phase Speed Estimates using Interferometry

To determine if a wave is responsible for an observed acceleration we need to know its phase velocity $\mathbf{v}_{\mathrm{ph}}$. There are several ways to determine the phase velocity of a wave. For example, the timing method above can be used if the wave is observed by several spacecraft. However, the wave might not be large enough and stable long enough to be observed at different spacecraft. If that is the case the interferometry method using a spacecraft's electric field probes could work. Figure 7.6 illustrates the concept of the method. Each probe in the spin-plane give simultaneous spatially separated measurements. One can combine these measurements to form electric field measurements in the same direction in two separate points, thus, allowing interferometry calculation. For example, two electric field measurements can be derived from: one, the potential difference between probe 1 and the average potential of the probes in perpendicular direction to 1 $(V_{p1} - (V_{p3} + V_{p4})/2)$ and two, in the same manner as before $((V_{p3} + V_{p4})/2 - V_{p2})$. If the observed wave is stable over the time it crosses the spacecraft, the two electric fields should be about the same with a time delay Δt (Fig. 7.7b).

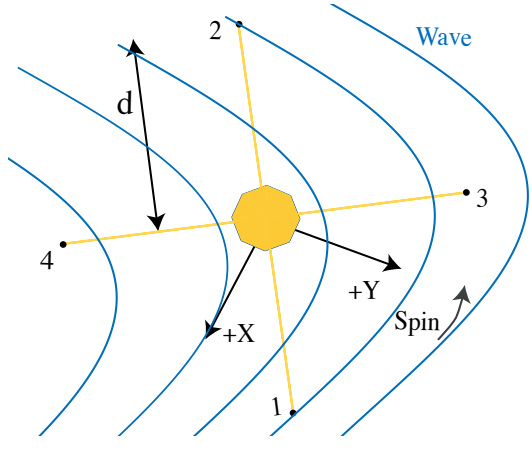

Figure 7.6. Illustration of the wave method.

Typically, a wave is composed of a range of frequencies f and interferometry method can be applied to each of these frequencies. In frequency space the phase difference $\Delta\gamma$ at a specific frequency is $\Delta\gamma = 2\pi f \Delta t$. From the phase difference one can derive the wave phase velocity for a specific frequency. This method is the equivalent to the timing method only it is done in frequency space. Furthermore, one can plot a frequency-wavenumber power spectrum like in Fig. 7.7c and also obtain a dispersion relation for the wave.

In Article III we determined that the waves were propagating parallel to the magnetic field, so when calculating the wave's electric field we used the probe pair most closely aligned with the magnetic field. The wave number $k_{\parallel}$ for a specific frequency was determined from $\Delta\gamma/(d\cos(\theta))$, where d, θ is the

separation between the two electric field measurements and angle between the probe pair and the magnetic field, respectively. Figure 7.7 shows results from one of the wave emissions observed in Article III. In Fig. 7.7c we see that the maximum of the power spectrum is located in an approximately linear line. Thus, we used a linear dispersion relation like in Graham et al. (2016b) over the maximum power frequency range, and obtained a phase speed of 207 km s^{-1} for this wave emission.

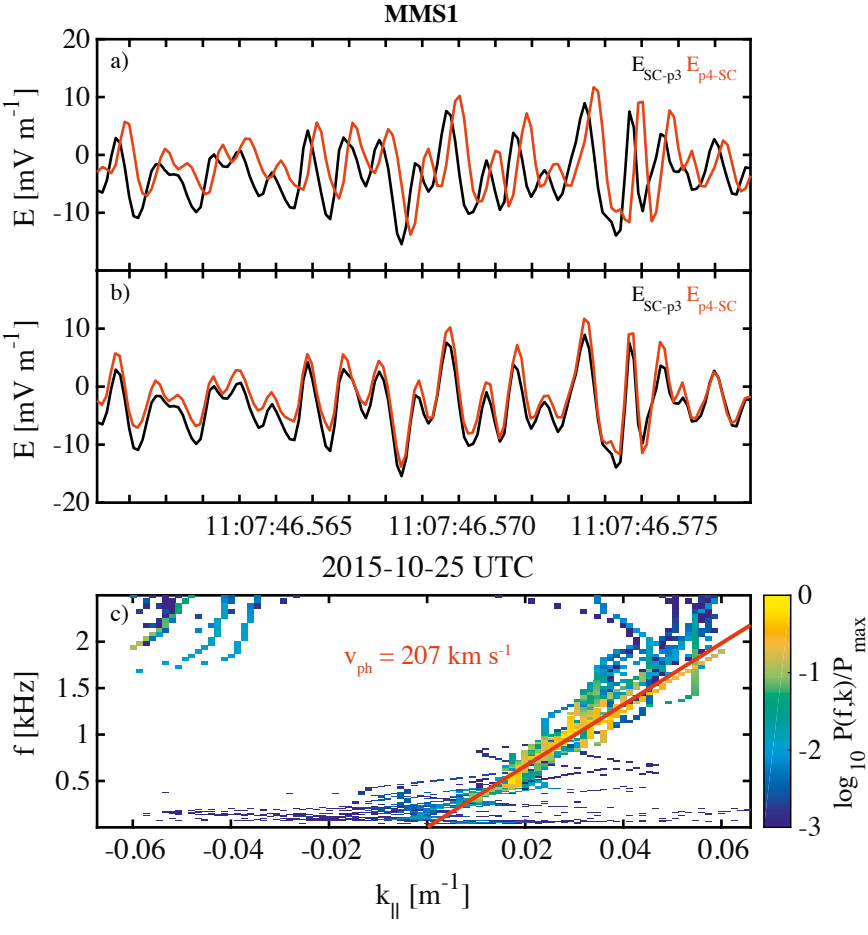

Figure 7.7. Data example showing the interferometry method from Article III (Eriksson et al., 2018). Panels a)-b) show the electric field derived from probe pair 34 where the electric field in b) is timeshifted by 0.26 ms corresponding to $v_{ph} = d\cos(\theta)/\Delta t =$ 207 km s^{-1} with $\theta = 25°$. c) frequency-wave number power spectrum obtained from $\mathbf{E}_{SC-p3}$ and $\mathbf{E}_{p4-SC}$, where $SC = (V_{p1} - V_{p2})/2$.

7.6 Liouville Mapping

The best way to determine which mechanism is accelerating a particle is by using Liouville's theorem. This is an important plasma theorem that states that a particle's distribution function is constant along the particle's trajectory, $f(\mathbf{r},\mathbf{v},t) = f(\mathbf{r}',\mathbf{v}',t')$. Thus, we can determine which acceleration mechanism (chapter 8) is occurring by mapping different points along the particle's trajectory. This is what is typically referred to as Liouville mapping. Note, this method requires an understanding of the acceleration region's field geometry and the particle trajectory in it. For example, if you have a parallel acceleration mechanism like a potential difference (chapter 8.3) the Liovuille mapping in the ideal case would be done between two spacecraft along the same field line. Detailed information regarding Liouville mapping can be found in e.g., Schwartz et al. (1998).

In this thesis we use Liouville mapping to study parallel electron acceleration. Figure 7.8 shows Liouville mapping from Article III; the black line shows the distribution function taken from a point along a field line where no acceleration was observed, the so called background population; the red dots show the energized distribution function taken from the time step given at the top of the figure; the green line gives the result of the Liouville mapping where the background population has been moved through a potential difference $\Delta\Phi_{\parallel}$. As can be seen in the figure, the red dots and green line agree very well, indicating that the observed energized electrons have been accelerated by a potential difference.

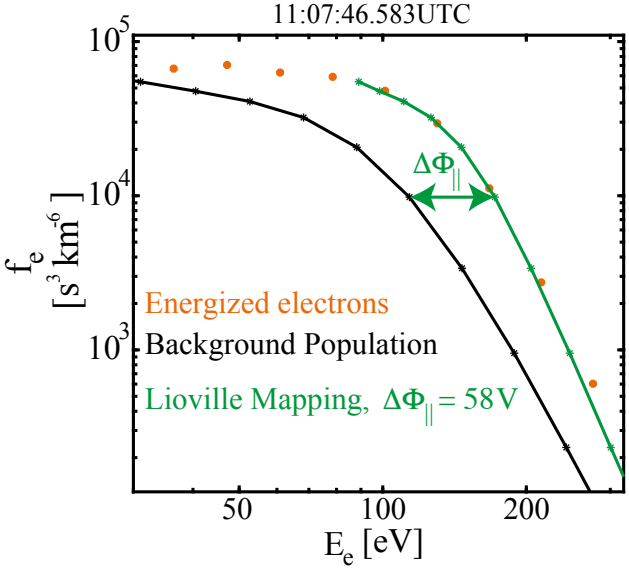

Figure 7.8. Example of Liouville mapping from Article III (Eriksson et al., 2018).

7.7 Acceleration Mechanisms

In the guiding-center approximation there are three fundamental acceleration mechanism capable of energizing electrons in reconnection: localized parallel electric field, Fermi acceleration, and betatron acceleration. An introduction to each of these mechanisms can be found in chapter 8. The change in the total electron kinetic energy density U due to these three fundamental mechanisms can be estimated as (Northrop, 1963; Dahlin et al., 2014):

$$\frac{dU}{dt} = \frac{p_\perp}{|\mathbf{B}|}\left(\frac{\partial|\mathbf{B}|}{\partial t} + \mathbf{u}_E \bullet \nabla|\mathbf{B}|\right) + (p_\parallel + m_e n_e u_\parallel^2)\mathbf{u}_E \bullet \boldsymbol{\kappa} + E_\parallel J_\parallel, \tag{7.7}$$

where $\mathbf{B}$ is the magnetic field, $\boldsymbol{\kappa} = \mathbf{b} \bullet \nabla \mathbf{b}$ is the magnetic field curvature, $\mathbf{b} = \mathbf{B}/|\mathbf{B}|$, $\mathbf{u}_E = (\mathbf{E} \times \mathbf{B})/B^2$, $u_\parallel$ is the electron bulk velocity parallel to $\mathbf{B}$, n_e is the electron density, $p_\parallel$, $p_\perp$ is the parallel and perpendicular electron pressures to $\mathbf{B}$, respectively, and $J_\parallel$ and $E_\parallel$ are the current density and electric field parallel to $\mathbf{B}$. The first term on the r.h.s. of equation 7.7 corresponds to the power density (energy transferred to electrons) due to betatron acceleration $\mathrm{W_{Betatron}}$ (section 8.1) where the term in the parentheses is $\sim dB/dt$, the second term corresponds the power density due to Fermi acceleration $\mathrm{W_{Fermi}}$ (section 8.2), and the last term corresponds to the power density due to acceleration by a parallel electric field $\mathrm{W_{E_\parallel}}$ (section 8.3 or 8.4). All the quantities on the r.h.s of equation 7.7 can be measured using MMS multi-spacecraft data and thus the power density of the different acceleration mechanisms can be experimentally estimated.

In Article IV we estimate the power density due to Fermi acceleration, betatron acceleration, and acceleration due to parallel electric fields in an outflow region of magnetotail reconnection with a tailward flow, see Figure 7.9. During the interval MMS crosses the center of the current sheet ($B_x = 0$ dashed magenta lines in Fig. 7.9a) three times. For the whole event the largest component of the ion velocity, $\mathrm{V_{ix}}$, is large and negative suggesting that MMS is crossing an outflow region with a tailward flow. During each crossing of the center of the current sheet $\mathrm{W_{Fermi}} > 0$ (Fig. 7.9c), consistent with what is expected from a simple 2-D picture of an outflow region (Fig. 7.9f). For each crossing of the current sheet we observe $\mathrm{W_{Betatron}} > 0$ close to the center of the current sheet (Fig. 7.9d). Around each positive peak in $\mathrm{W_{Betatron}}$ we observe regions of negative $\mathrm{W_{Betatron}}$. This is consistent with MMS being closer to the separatrix regions where the magnetic field magnitude decreases as electrons drift towards the center of the current sheet. All these observations are consistent with MMS moving in the manner shown in green in the sketch in Fig. 7.9f. Finally, $\mathrm{W_{E_\parallel}}$ (Fig. 7.9e) has the lowest values of all three acceleration mechanisms. However, the observational uncertainties in $\mathrm{W_{E_\parallel}}$ (marked yellow), caused by the uncertainties in the parallel electric field measurement, is larger than the $\mathrm{W_{E_\parallel}}$ magnitude. Thus, no further conclusions regarding $\mathrm{W_{E_\parallel}}$ can be drawn. Comparing the different mechanisms we see that $\mathrm{W_{Fermi}}$ has the largest peaks and average value of all three mechanisms,

suggesting that Fermi acceleration is the most efficient accelerator of electrons during the event.

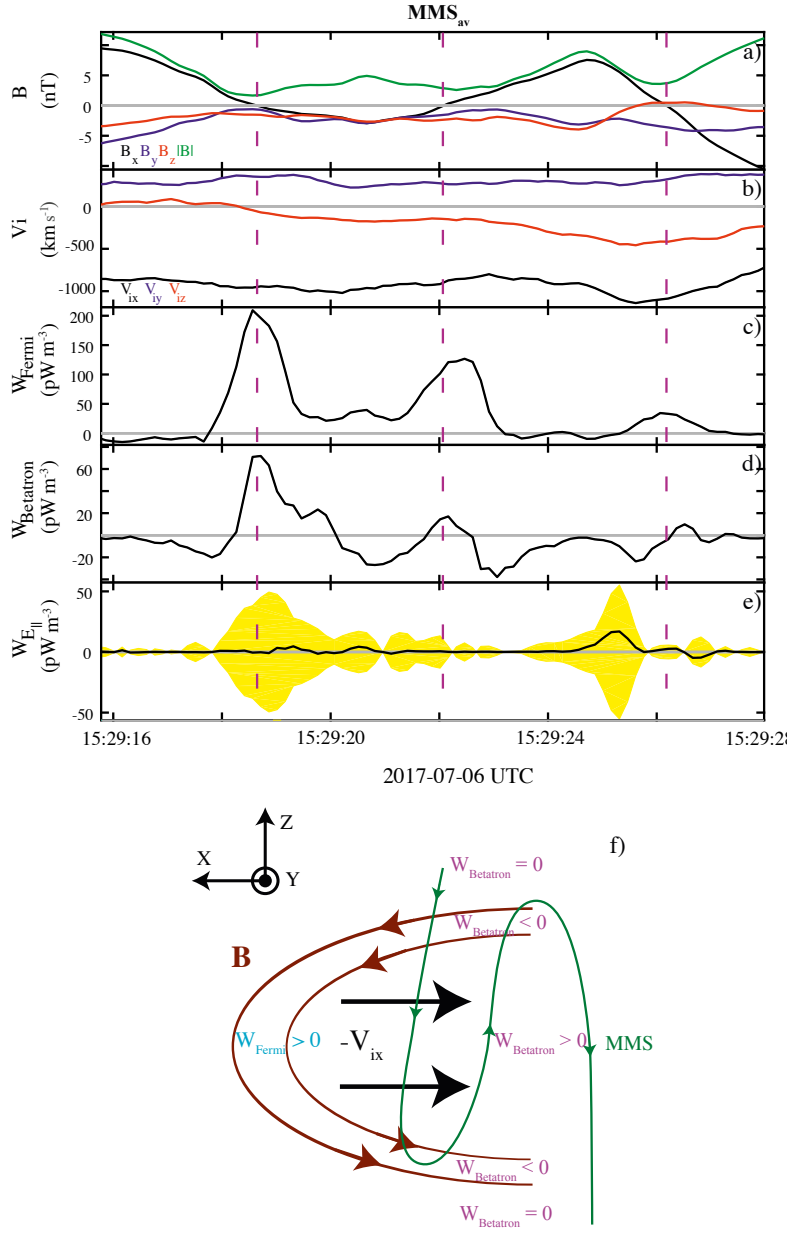

Figure 7.9. Results from Article IV where a) the magnetic field, b) ion bulk velocity, c) W_{Fermi}, d) $W_{Betatron}$, e) $W_{E_{||}}$, where the yellow shaded area indicate the observational uncertainties in $W_{E_{||}}$, f) simple 2-D sketch of a reconnection tailward outflow region, where the green line indicate the trajectory of MMS across the outflow region. The magenta dashed lines in panel a-e) indicates the crossings of the CS center.

8. Electron Acceleration Mechanisms

In this chapter we give a brief introduction to four fundamental acceleration mechanisms used in this thesis: betatron acceleration, Fermi acceleration, acceleration by potential difference, and wave-particle interaction. Observations of one acceleration mechanism does not mean that the others are not contributing to the final energy gain. Indeed, when you look at complex processes such as shocks and reconnection it is usually several mechanisms occurring simultaneously. Thus, when investigating possible acceleration mechanisms a number of different combinations needs to be considered.

For particles to be accelerated, the energy needs to come from somewhere. In the outer magnetosphere, the gravitational forces can be neglected and therefore charged particles only gain energy from electromagnetic forces. The equation of energy conservation (the Poynting theorem)

$$\mathbf{E} \cdot \mathbf{J} = -\frac{\partial}{\partial t}\left(\frac{1}{2}\epsilon_0 E^2 + \frac{1}{2\mu_0} B^2\right) - \nabla \cdot \mathbf{S}, \tag{8.1}$$

states that energy is transferred into plasma energy from electromagnetic field energy when there is an electric field and current present. The term on the l.h.s of equation 8.1 indicates if energy is given to or received from the plasma. If $\mathbf{E} \cdot \mathbf{J} < 0$, energy is taken from the plasma, while $\mathbf{E} \cdot \mathbf{J} > 0$ means that energy is given to the plasma. The first term on the r.h.s gives the electromagnetic energy density and the second term $\mathbf{S} = (\mathbf{E} \times \mathbf{B})/\mu_0$, the so called Poynting vector, gives the electromagnetic energy flux. The work done on a charged particle is given by

$$W = \mathbf{F} \cdot \mathbf{v}. \tag{8.2}$$

Using the Lorentz force on an electron,

$$\mathbf{F}_L = -e\,(\mathbf{E} + \mathbf{v} \times \mathbf{B}), \tag{8.3}$$

it is clear that the acceleration of an electron only comes from an electric field. After all the force due to $\mathbf{B}$ is perpendicular to $\mathbf{v}$. Thus, to gain energy an electron needs to move antiparallel to $\mathbf{E}$ for all electron acceleration mechanisms. In the following subsections a summary of betatron acceleration, Fermi acceleration, potential difference, and Landau damping mechanism is given. Each mechanism can work on ions and electrons, however, this thesis is focused on electrons so we will only refer to electrons in the rest of the chapter.

8.1 Betatron Acceleration

Betatron acceleration is based on the conservation of the magnetic moment. The first adiabatic invariant, the magnetic moment, is given by:

$$\mu = \frac{\varepsilon_\perp}{|\mathbf{B}|}, \tag{8.4}$$

where $\varepsilon_\perp$ and $|\mathbf{B}|$ are the perpendicular energy and the magnitude of the magnetic field, respectively. The magnetic moment is constant if the electron motion is adiabatic, i.e., the scale of the electric and magnetic field changes observed by the electron is much larger than the gyroperiod (the time it takes an electron to gyrate one orbit around the magnetic field) and gyroradius (the radius of one orbit around the magnetic field). What this means is that if an electron moves from a lower $|\mathbf{B}|$ to a higher one the perpendicular energy must also increase, an example is shown in Fig. 8.3.

If there is no electric field in the system, the energy of the electron should be constant, and therefore the perpendicular energy increases as much as the parallel energy decreases. In this case the equation of conservation of magnetic moment (equation 8.4) tells us how the electron pitch angle α (the angle between the magnetic field and the electron's velocity) change as the electron moves between regions of different magnetic field magnitudes

$$\frac{sin^2(\alpha_1)}{sin^2(\alpha_2)} = \frac{B_1}{B_2}. \tag{8.5}$$

This is commonly referred to as magnetic mirroring and is, for example, the reason there are trapped energetic electrons in the radiation belts. As another example important for this thesis, magnetic mirroring is also the cause of the loss cone in the electron distribution functions that is commonly observed in the magnetosheath (MSH) downstream of the bow shock (Feldman et al., 1983). Figure 8.1 illustrates the theory behind the loss cone feature at a shock. A shock can have an overshoot, a localized region at the shock with a strong magnetic field, $B_{max} = |\mathbf{B}|$, that has higher magnitude than the magnetic field in the magnetosheath. Imagine that the magnetosheath (I) and solar wind (SW) (III) regions are each filled with a maxwellian distribution (blue and grey regions in velocity space figures, respectively, in Fig. 8.1). Magnetosheath electrons with a pitch angle less than $\alpha = sin^{-1}(\sqrt{B_{MSH}/B_{max}})$ will pass the overshoot and continue into the solar wind. Because these electrons are not reflected, there will be a gap in the magnetosheath population in the directions opposite to the electrons leaving into the solar wind, a so called loss cone. However, solar wind electrons with a pitch angle less than $\gamma = sin^{-1}(\sqrt{B_{SW}/B_{max}})$ will also cross the overshoot from the solar wind into the magnetosheath and fill the loss cone region of the magnetosheath population. Note that at the peak of the overshoot the loss cone is 90°. Solar wind electrons are significantly colder than magnetosheath electrons and as a consequence the electron distribution

function in the magnetosheath show a loss of electrons at higher energies while at the lower energies the incoming solar wind electrons are observed. Examples of such distribution functions are seen in Fig. 8.2 from Article II.

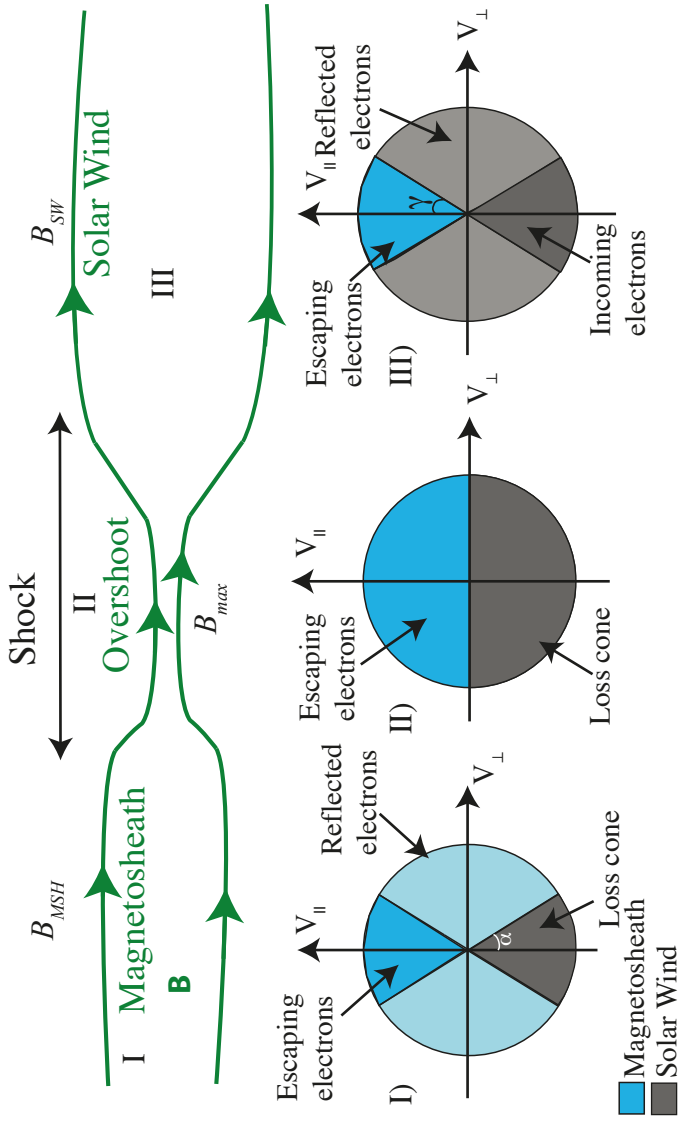

Figure 8.1. Sketch of the mechanism of loss cone. Green lines gives the magnetic field. I-III shows maxwellian distributions inside the different regions according to conservation of magnetic moment, where the blue color indicates the magnetosheath population and grey the solar wind population.

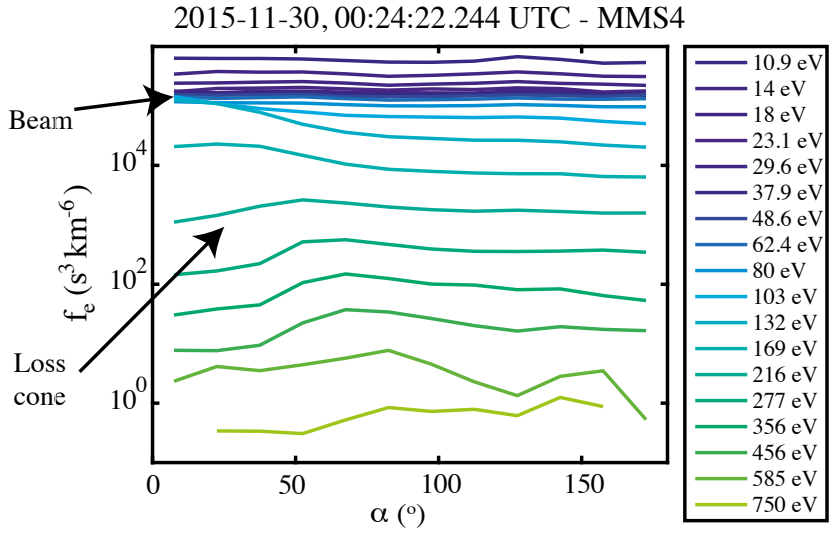

Figure 8.2. Detailed plot of the energized electron pitch angle distribution function shown in Article II (Eriksson et al., 2016), where the different energies are given by the color of the lines. The black arrows points out the loss cone and beam features.

If there is an electric field in the system, then the total energy of an electron can change. In that case, if the magnetic field increases as the electron drifts, both the perpendicular as well as the total velocity of the electron will increase (see Fig. 8.3). Of course, this also means that you can get deceleration, betatron cooling, if the electron drifts from a region with higher magnetic field to a lower one. Betatron acceleration is usually observed in space as an increase in the plasma temperature perpendicular to the magnetic field (Fig. 8.4II). The state where $T_{\perp,e} >> T_{\parallel,e}$ is unstable and emissions of plasma waves, usually whistler waves (Khotyaintsev et al., 2011), will transport the energy from the perpendicular direction to the parallel one. Betatron acceleration is believed to be one of the primary electron acceleration mechanisms at the dipolarization fronts near Earth (Fu et al., 2011; Birn et al., 2012; Turner et al., 2016; Birn et al., 2013, e.g.,) and has also been observed at Mercury (Dewey et al., 2017).

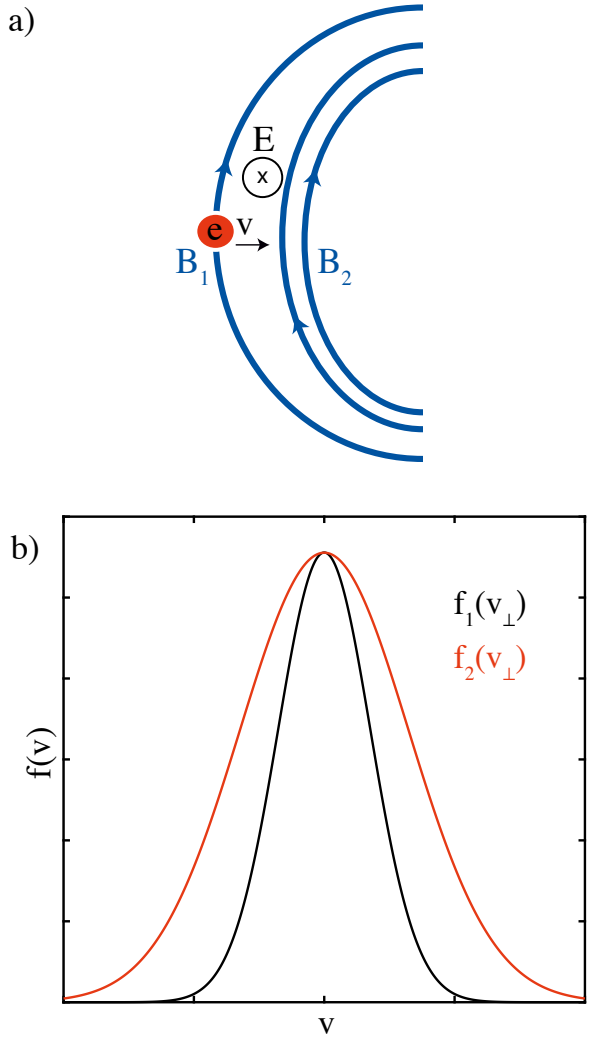

Figure 8.3. Betatron acceleration. a) simple sketch of betatron acceleration at a dipolarization front where the blue lines are the magnetic field lines and the black arrow gives the electron drift velocity. b) how the distribution function changes due to betatron acceleration assuming a maxwellian distribution function.

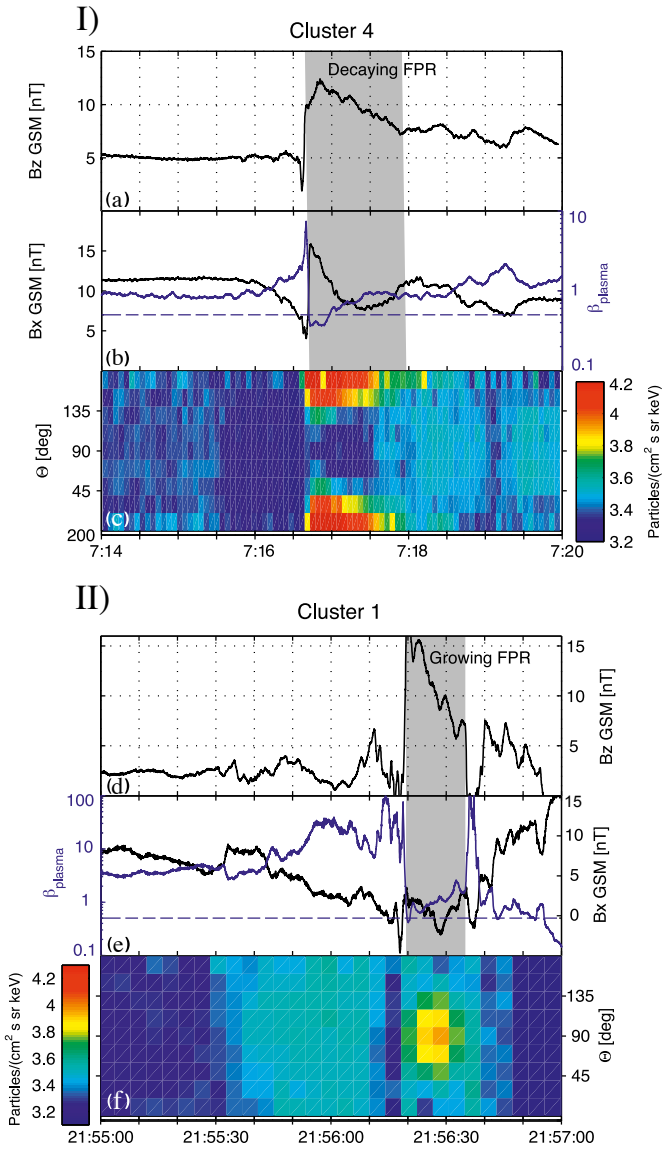

Figure 8.4. Example of Fermi and betatron electron acceleration seen at a dipolarization front in near-Earth space. I) Example of Fermi electron acceleration observed on 3 September, 2006. The signature can be seen in panel c). II) Example of betatron electron acceleration observed on 1 October, 2007. The signature can be seen in panel f). The different panels shows: a) and d) Z component of the magnetic field in GSM coordinates. b) and e) the black curves represents X component of the magnetic field in GSM coordinates and the blue lines the plasma beta. c) pitch angle distribution of the 4068 keV electrons and f) pitch angle distribution of 40-400 keV electrons. The grey area indicate the region where the accelerations are observed. Adapted from Fu et al. (2011).

8.2 Fermi Acceleration

Fermi acceleration is an acceleration process that occurs in many different astrophysical environments. It has been shown with in-situ measurement to be one of the primary electron acceleration mechanism at the dipolarization fronts at Earth (e.g., Birn et al., 2012; Birn et al., 2013) and Mercury (Dewey et al., 2017). It is also important for electron acceleration in reconnection as shown in simulations (e.g., Dahlin et al., 2016), direct observations from Earth (e.g., Birn et al., 2012; Turner et al., 2016, and references therein), and remote observations from solar flares (e.g., Benz, 2016) and gamma-ray structures believed to be involved in acceleration of galactic cosmic rays (Chernyshov et al., 2017). Fermi acceleration is based on the conservation of the second adiabatic invariant, J. The second adiabatic invariant is given by

$$J = m \int_1^2 u_{\parallel} ds = 2ml \langle u_{\parallel} \rangle, \tag{8.6}$$

where l is the total length of the magnetic field between two mirror points. If the mirror points are from a magnetic mirror, the second adiabatic invariant can only be conserved if the first adiabatic invariant is conserved. The second invariant means that if an electron travels along a convecting field line as in Fig. 8.5a the decrease in l will result in an increase in the average parallel energy of the electron (Fig. 8.5b) (Birn et al., 2012). Thus, an electron can gain energy by bouncing back and forth on a convecting field line. Fermi acceleration is usually observed in space as an increase of electron temperature in the direction parallel to the magnetic field (Fig. 8.4I).

In Article IV we look at the power density of Fermi acceleration, betatron acceleration, and acceleration due to a parallel electric field (section 7.7) inside a tailward outflow region in the magnetotail. We show that Fermi acceleration is the dominant electron acceleration mechanism during the studied event (see Figure 7.9).

8.3 Acceleration by Potential Difference

Electrons can also be directly accelerated by a parallel electric field. The parallel electric field in this section comes from a potential difference $\Delta\Phi_{\parallel}$ along the magnetic field. Electrons encountering a local potential difference between two points along a magnetic field line

$$\Delta\Phi_{\parallel} = \int_1^2 E_{\parallel} dl, \tag{8.7}$$

can be accelerated or decelerated depending on the direction of the electrons and the electric field (Fig. 8.6). Compared to Fermi and betatron acceleration, where the energy gain depends on the particle energy, in the case of acceleration

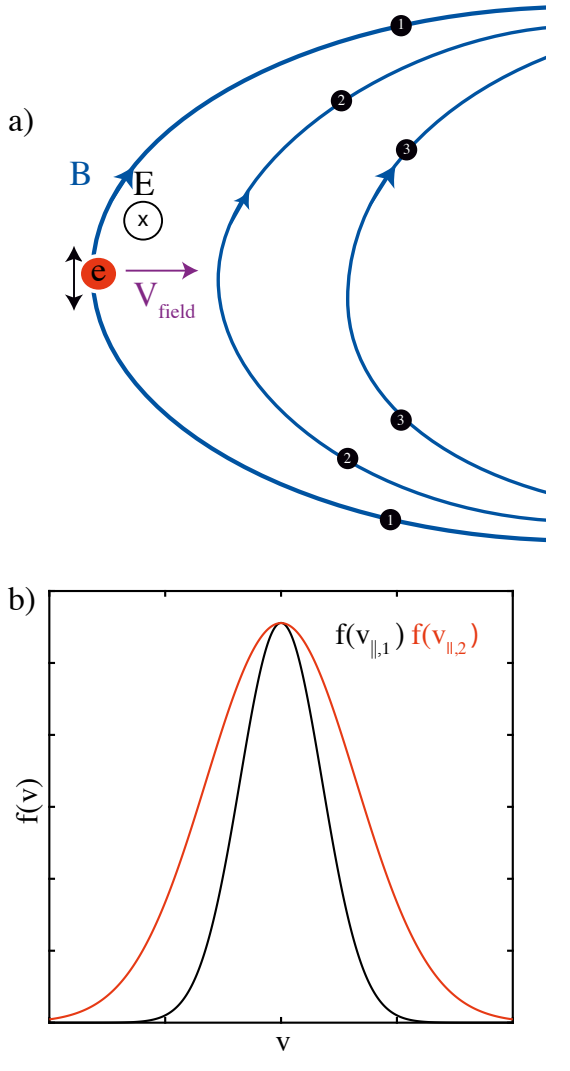

Figure 8.5. Fermi acceleration. a) simple sketch illustrating Fermi acceleration in an outflow region of reconnection where the blue lines show the convecting magnetic field, the black arrow indicates the electron motion, $\mathbf{V}_{\text{field}}$ is the velocity of the convecting field lines, and the numbered black dots indicate the reflection points at different times. The length of the field line between the reflection points give l. b) illustration how the distribution function changes for multiple bounces of Fermi acceleration, assuming a maxwellian distribution.

by a potential difference all particles gain the same energy (maximum $e\Delta\Phi_{\parallel}$). This implies that the relative change in energy is higher for low energy particles,

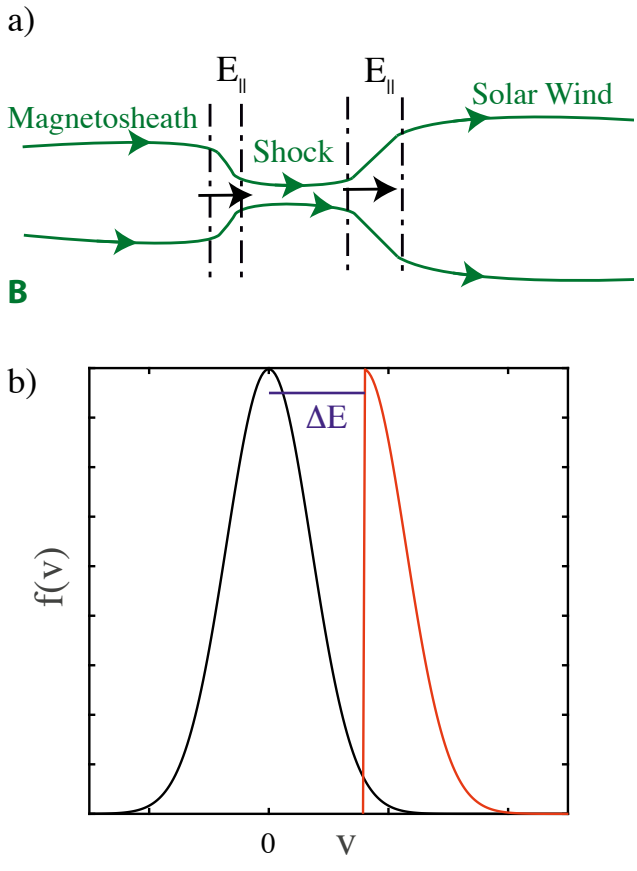

Figure 8.6. Acceleration by a potential difference. a) simple sketch illustrating acceleration by a potential difference at a bow shock where the green lines indicate magnetic field and $E_{\parallel}$ is the electric field parallel to the magnetic field. Electrons moving antiparallel to the magnetic field will be accelerated. b) example of changes to the distribution function due to the acceleration by a potential difference assuming maxwellian distribution functions where ΔE is the energy increase,

thus, the energy gain for this acceleration mechanism will be more apparent at lower energies.

Acceleration by $\Delta\Phi_{\parallel}$ has been shown to be responsible for electron acceleration observed directly in reconnection (e.g., Birn et al., 2012; Graham et al., 2014; Graham et al., 2016a; Eriksson et al., 2018), at the Earth's bow shock (e.g., Feldman et al., 1983), and indirectly at solar flares (Benz, 2016, and references therein).

In Article III we show an example of electron acceleration by a potential difference. The acceleration mechanism and corresponding potential difference is determined with the help of Liouville mapping, see Fig. 7.8. We also

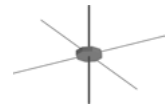

observe a locally accelerated electron beam due to a potential difference in Article II (Fig. 8.2).

8.4 Wave-Particle Interaction

Wave-particle interaction is another common electron acceleration mechanism in space. It has been observed directly at the Earth's bow shock (e.g., Oka et al., 2017), at Saturn's bow shock (Masters et al., 2016), Jupiter's auroral region (Mauk et al., 2017), in the Earth's magnetosphere (Birn et al., 2012, and references therein), in-directly at solar flares (Benz, 2016, and references therein), and in simulations (e.g., Watt and Rankin, 2008).

One example of wave-particle interaction that can increase energy and was relevant to Article III is Landau damping (Swanson, 1989). It occurs when some of the electrons are in resonance with an electrostatic wave; their speed, v, is about the same as the phase speed, v_{ph}, of the wave. If more of the electrons have velocities slightly below the wave phase velocity, the wave will damp and energy will be transferred from the wave to the electrons (Fig. 8.7). This will result in a restructuring of the distribution function like shown in red in Fig. 8.7. However, the opposite is also true. If more of the electrons have velocities slightly above the phase velocity of the wave, then the electrons will lose energy and the wave will grow. To determine if a wave is responsible for an observed electron acceleration you need to determine the direction **k** and the potential of the wave. These properties help determine which electrons the wave can interact with.

In Article III, where we could estimate the direction and potential of waves, we determined that waves were not an important accelerator of the observed energized electrons.

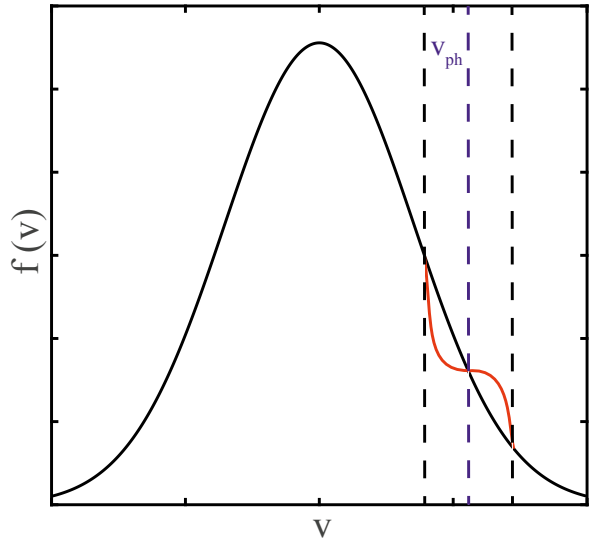

Figure 8.7. Sketch of the Landau damping effect assuming maxwellian distribution. The blue dashed line indicate the phase speed of the wave. The black dashed lines indicate the potential of the wave, the regions of electrons affected by the wave. The red line indicate the change in the distribution function due to wave-particle interaction.

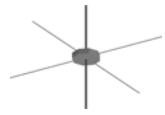

9. Looking to the Future

This thesis is just one step forward in trying to understand electron acceleration and heating in space. There are still many more questions to answer related to the results in the articles in this thesis. For example, related to Article I a recent simulation (Olshevsky et al., 2016) and observational (Fu et al., 2017) study has determined that spiral nulls are more important for energy dissipation than the radial nulls. Both of these studies determined the null's type from linear interpolation (equation 5.1). However, they did not consider magnetic field fluctuations despite being performed in a turbulent plasma. As we showed in Article I magnetic null identification is very sensitive to localized magnetic field fluctuations. Thus, the magnetic field from these studies should be looked at to determine if the turbulence has in any way affected the type identification. If not then this study will strengthen their conclusions that spiral nulls are sites of large energy dissipation. It is also important to determine what is the relative contribution of nulls to electron energization. To determine the importance of magnetic nulls compared to other processes in turbulent plasmas. Are nulls the biggest dissipators? Are waves more involved in the heating of the plasma or just scattering from non-adiabatic motion? Currently, there is a lot of burst data available from MMS in the turbulent magnetosheath that could be used for this study.

Another important step is to make a statistical study over the actual acceleration mechanisms and if possible where they are taking place in the magnetosheath. Chasapis et al. (2017) showed correlation between heating and the strength of current regions and something similar should be done for the electron acceleration mechanisms, since MMS has enough resolution to resolve them. In Article III we presented a reconnecting current sheet, while the current region in Article II was too complex to determine if it was reconnecting (at least according to the traditional 2-D picture). Both current sheets were most likely generated by the velocity shear from a magnetosheath jet, so why was one reconnecting and the other was not? Is the current sheet in Article II going to reconnect later or is it some other condition that stops the reconnection process from occuring? Or is the current sheet in Article II reconnecting in a way not covered by traditional theory? The best way to try to answer these questions is through a statistical study over current sheets at magnetosheath jets and their properties and compare with simulations of magnetosheath jets/velocity shear current sheets. Both Article II and III have a similar electron acceleration mechanism so it would be important to see if all current sheets at magnetosheath jets show the same electron acceleration

mechanism in the statistical study. If the acceleration mechanism could be a characteristic of thin current sheets created by magnetosheath jets. In Article III we presented an in-depth study of electron acceleration mechanism at a reconnecting magnetosheath current sheet. This study should be continued by looking at more reconnecting magnetosheath current sheets and their related electron acceleration. In Wilder et al. (2018) several reconnection events with different guide-fields in the magnetosheath are listed. This list could be used as a starting point for looking at electron acceleration at reconnecting magnetosheath current sheets and see if the acceleration changes based on the guide-field strength by estimating the power density of different acceleration mechanisms like in Article IV.

In Article IV we looked at electron acceleration in a tailward outflow region in the magnetotail. This study should be continued by repeating it over more data when MMS are in the magnetotail to determine if our conclusions are just for this particular event or is more general for magnetotail reconnection. It should also be performed in other plasma regions like the magnetopause and the magnetosheath, like mentioned above, to determine if different plasma conditions change the conclusions regarding the acceleration mechanisms. There was also several interesting structures observed in the MMS data on July 6th 2017, such as an X-line reversal with normal direction in GSE_X, that needs to be looked at in detail.

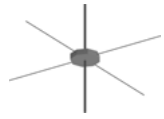

10. Article Summaries

Here follows a summary of all articles included in the thesis, together with a description of the contribution made by the author of this thesis to each publication.

10.1 Summary of Article I

Statistics and accuracy of magnetic null identification in multispacecraft data

---

Authors

E. Eriksson, A. Vaivads, Yu. V. Khotyaintsev, V. M. Khotyayintsev, and M. André

Journal

Geophysical Research Letters (GRL)

Details

Volume 42, Issue 17, 2015, Pages 7

My Contribution

I performed the data analysis and wrote the article, with valuable contributions from the co-authors in the form of discussions and comments on the original manuscript. Yu. V. Khotyaintsev and V. M. Khotyayintsev also derived the theoretical minimum disturbance capable of changing the null type between A and B kind (δB_2).

Summary

In Article I, we perform the first statistical study of magnetic nulls in the Earth's nightside magnetosphere. Magnetic nulls, regions of vanishing magnetic field, is one way to characterize 3-D magnetic topologies and are believed to be

important in 3-D reconnection and turbulence. In the vicinity of a null, plasma particles become unmagnetized and can be accelerated to high energies by electric fields. In this article we use the two available multi-spacecraft methods (Poincaré index PI and Taylor Expansion TE) to locate the magnetic nulls using magnetic field data from Cluster from July 2003 to January 2004 when the spacecraft are in the nightside magnetosphere. Figure 10.1 shows the location of all identified nulls using the two location methods. More nulls are located at the magnetopause than in the magnetotail current sheet, due to the orbit and the dynamic nature of the magnetopause, resulting in many more crossings of the magnetopause. The TE method also find more nulls than the PI method, which is expected since the box volume used with TE is much larger than the spacecraft tetrahedron used for PI. 80 % of the observed nulls are type-identified as spiral nulls, which is very close to what we obtain when forming a fully random magnetic field, suggesting that the physical processes behind null formation do not favour any particular type of nulls.

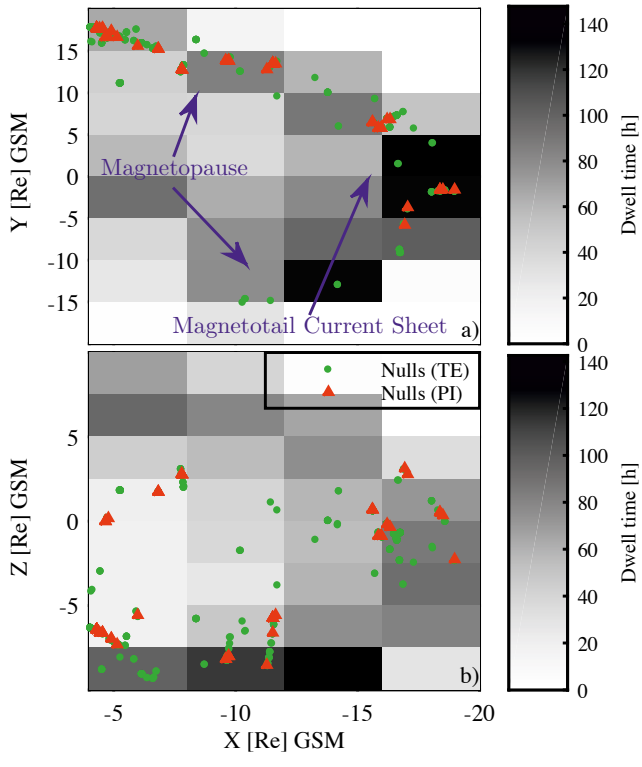

Figure 10.1. The results from the statistical study in Article I (Eriksson et al., 2015). Each symbol gives the position of the magnetic nulls found for both the Poincaré index (PI), red triangle, and Taylor Expansion (TE) method, green circle, in GSM coordinates. The gray background gives the dwell time of the spacecraft in each of the spatial bins.

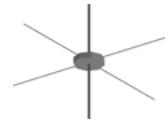

The magnetic topology around a magnetic null can be different. The magnetic topology of a null determines what kind of plasma processes such as reconnection can occur at it (Birn and Priest, 2007). A null's type describes the magnetic topology around the null. Thus, being able to accurately determine the type of an observed null is important. When looking over the results from the statistical study we notice for some events the magnetic null type change rapidly. One of those events is shown in Fig. 10.2, where the null type is given by the red triangle symbols in panels d)-f). This made us look at what effect local magnetic field fluctuations have on the identification of nulls, since magnetic field fluctuations is common in many regions in space. Usually, large fluctuations in magnetic field data originate from local plasma processes (e.g., waves or localized structures on spatial scales smaller than the spacecraft separation), but can also be due to instrumental errors. We show that the characterization of magnetic nulls is sensitive to local fluctuations in the magnetic field. We also develop and demonstrate a method for determining how reliable the magnetic null characterization is. Using typical errors (instrumental + local fluctuations) of 1 nT we show that 70% of the nulls in the statistical study have a well-defined type. In conclusion, nulls are common at the nightside magnetosphere and the magnetic null characterization can be affected by magnetic field fluctuations. Thus, the effect of magnetic field fluctuations should be considered before making statements based on a null's type.

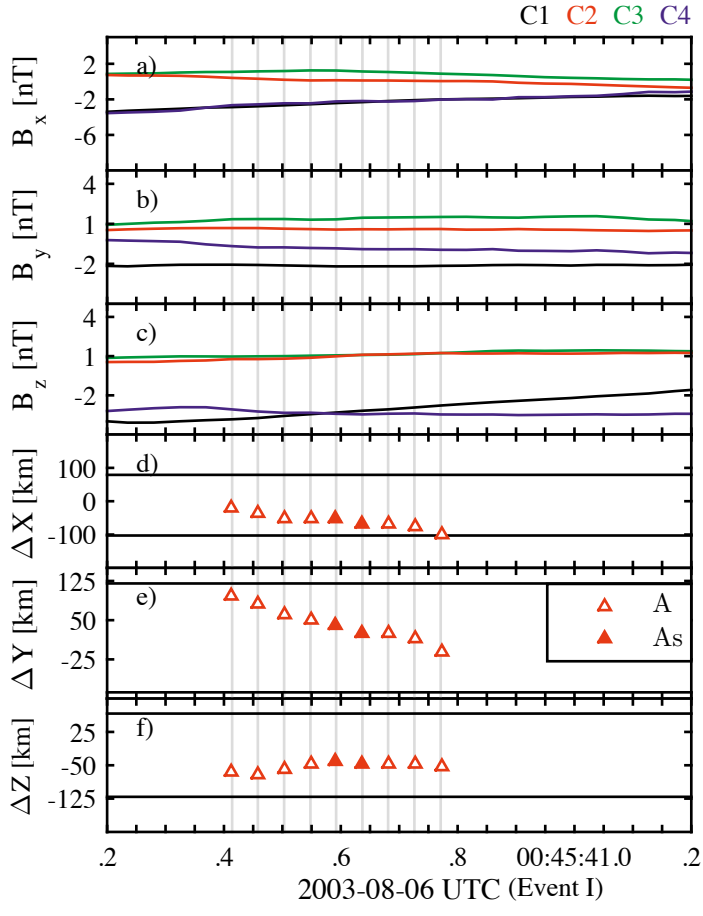

Figure 10.2. An example of magnetic null observations from Article I (Eriksson et al., 2015) using TE method. a)-c) show the magnetic field components in GSM for all four Cluster spacecraft. d)-f) show the distance to the magnetic null from the center of the four spacecraft, the mean value of all the spacecraft positions. The straight black lines indicate the edges of the spacecraft box volume. The type of the null is given by the symbols in d)-f).

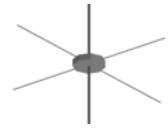

10.2 Summary of Article II

Strong current sheet at a magnetosheath jet: Kinetic structure and electron acceleration

Authors

E. Eriksson, A. Vaivads, D. B. Graham, Yu. V. Khotyaintsev, E. Yordanova, H. Hietala, M. André, L. A. Avanov, J. C. Dorelli, D. J. Gershman, B. L. Giles, B. Lavraud, W. R. Paterson, C. J. Pollock, Y. Saito, W. Magnes, C. Russell, R. Torbert, R. Ergun, P- A. Lindqvist, and J. Burch

Journal

Journal of Geophysical Research: Space Physics (JGR)

Details

Volume 121, Issue 10, 2016, Pages 11

My Contribution

I planned the study, performed the data analysis, and wrote the article, with valuable contributions from the co-authors in the form of discussions and comments on the original manuscript.

Summary

In Article II we present observations from an ion-scale current sheet in the turbulent magnetosheath downstream of the quasi-parallel bow shock. In the turbulent magnetosheath electrons are efficiently heated (Retinò et al., 2007; Chasapis et al., 2015) and electrons accelerated to suprathermal energies have been observed there (Retinò et al., 2007). Simulations suggest that a possible generator of thin current sheets in this turbulent region can be localized dynamic pressure enhancements often called magnetosheath jets (Karimabadi et al., 2014; Hao et al., 2016; Omidi et al., 2016). We show observations that suggest that the studied current sheet is forming due to high velocity shears associated with a magnetosheath jet (purple regions in Fig. 10.3a). Earlier studies have shown local shocks forming in regions of magnetosheath jets (Hietala et al., 2009). However, the estimated magnetosonic Mach number in the current sheet's reference frame during the current sheet crossing is much lower than 1 indicating that this current sheet is not a localized shock. There is also no clear signatures of ongoing reconnection at the current sheet. However, we cannot

exclude the possibility that the sub-ion scale structures observed within the current sheet is due to for example flux rope formation during reconnection. It can even be that the current sheet starts reconnecting later as it propagates deeper into the magnetosheath.

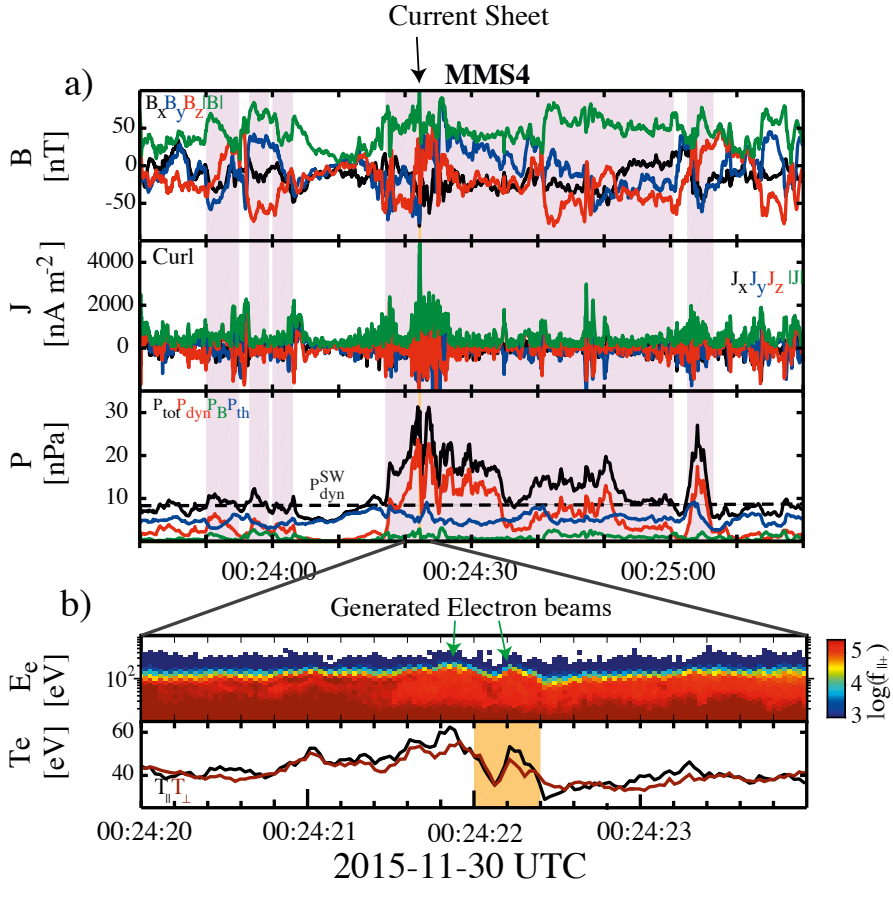

Figure 10.3. a) Overview of the result from Article III (Eriksson et al., 2016) showing the current sheet (orange area) at a local magnetsheath jet (purple color) boundary where P_{dyn} rapidly changes. The panels from top to bottom correspond to the magnetic field, current density, and pressure, respectively, where the dashed black line indicate the solar wind dynamic pressure. b) electron distribution function parallel and electron temperature parallel and perpendicular to the magnetic field, respectively, where the locally generated electron beams are marked by green arrows.

Observations suggest electron heating and beam formation parallel to the magnetic field right before and inside the current sheet (Fig. 10.3b). Parallel electron beams are observed continuously in the interval (top panel in Fig. 10.3b), indicating a parallel acceleration mechanism. Despite the continuous

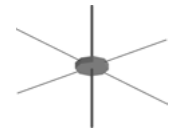

observation of beams along the whole interval we believe the electron beam right before and inside the current sheet are being locally accelerated. There are two main reasons why we believe the electron beams are locally accelerated. First, for acceleration to occur a parallel electric field is required. The strong field-aligned current in the center of the current sheet suggest the possibility of such a parallel electric field. Secondly, the other beams observed in the interval (top panel in Fig. 10.3b) are more diffused than the beams inside and right before the current sheet crossing. More diffused beams are expected to have formed somewhere else. The electron beam inside the current sheet is observed between ~ 80 and 120 eV confined to pitch angles less than about 45° (Fig. 8.2). At energies above the beam energy we observe a loss cone consistent with part of the electrons from the hotter magnetosheath-like side escaping into the colder solar wind-like plasma on the other side of the current sheet. All these observations fit well with the theory of electron acceleration proposed by Feldman et al., 1983 commonly used to explain electron acceleration across a shock due to a change in electrostatic potential. However, in our case the electron acceleration is occurring locally inside the magnetosheath. Therefore, electron beams observed in the magnetosheath do not have to originate from the bow shock like previously believed (e.g., Mitchell and Schwartz, 2013).

10.3 Summary of Article III

Electron Energization at a Reconnecting Magnetosheath Current Sheet

Authors
E. Eriksson, A. Vaivads, D. B. Graham, A. Divin, Yu. V. Khotyaintsev, E. Yordanova, M. André, B. L. Giles, C. J. Pollock, C. Russell, O. Le Contel, R. Torbert, R. Ergun, P- A. Lindqvist, and J. Burch

Journal
Geophysical Research Letters (GRL)

Details
Volume 45, Issue 16, 2018, Pages 10

My Contribution
I planned the study, performed the data analysis, and wrote the article, with valuable contributions from the co-authors in the form of discussions and comments on the original manuscript. Andrey Divin performed the simulation used in the article.

Summary

In Article III we present observations of electron energization at a sub-ion scale reconnecting current sheet located in the turbulent magnetosheath downstream the quasi-parallel bow shock. Not a lot is known regarding what happens at these small scales due to limited particle resolution from previous missions. However, with MMS we can finally try to understand what processes are responsible for the electron heating and acceleration at sub-ion scales. The current sheet contains signatures consistent with reconnection such as the narrowness of the current sheet (0.7 d_i), non-zero B_N, Hall magnetic field supported by electrons carrying the current, and electron heating parallel to the magnetic field. We do not observe any clear ion outflow jet, typically expected of reconnection, when crossing the current sheet. Comparisons with numerical simulation suggest that this is due to MMS crossing a current sheet extended for several d_i in the L direction near the X-line. However, it could also be because the ions are already decoupled and only electrons are reconnecting as suggested by Phan et al. (2018).

Localized heating and electron acceleration parallel to the magnetic field are observed when crossing separatrix regions. Parallel propagating electrostatic waves are observed in these regions. However, when determining the wave's phase speeds (210 and -250 km s^{-1}, respectively) and electrostatic potentials ($\leq$ 1 V) (Fig. 10.4) we conclude that the waves are too slow with too low potential to be responsible for the observed acceleration and heating. We speculate they are more likely a possible byproduct of the accelerated electrons through electron-electron instability or ion-electron instability.

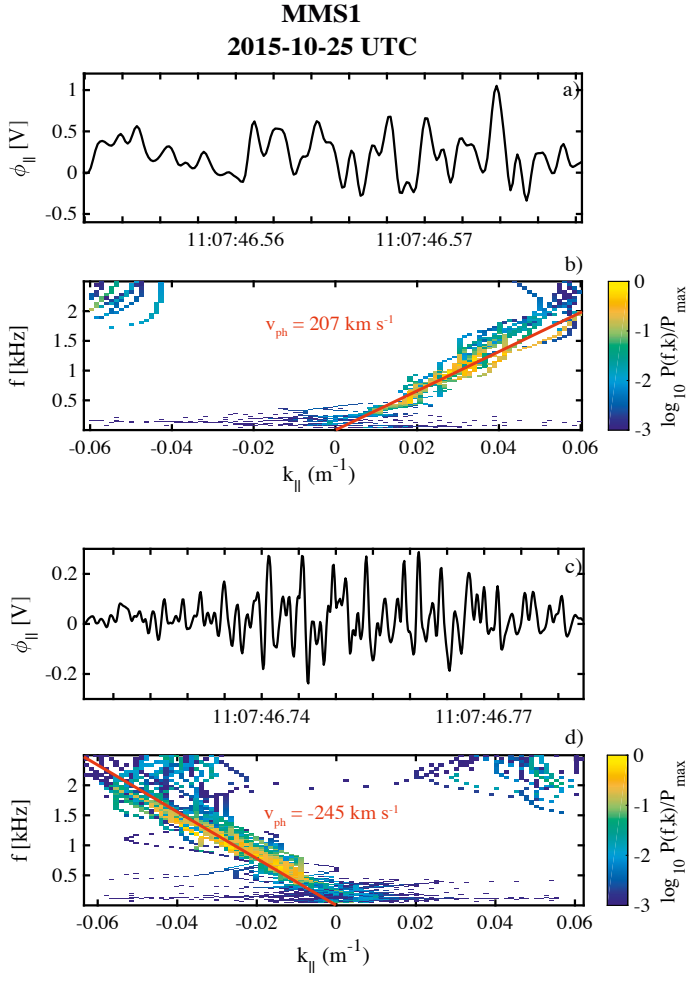

Figure 10.4. Electric field measurements from the wave emissions in Article III (Eriksson et al., 2018). a), c) electrostatic potential for the waves, b), d) wave number-frequency power spectrums derived using interferometry method showing the estimated wave speeds from a fit to a linear dispersion relation.

Using Liouville mapping (Fig. 7.8) on electron distribution functions we show that the energized electrons correspond to an acceleration from a potential difference $\Delta\Phi_{\parallel}$. The observed electron heating is found to be a fraction of $\Delta\Phi_{\parallel}$. We also get a similar value to the observed potential difference, when calculating the predicted $\Delta\Phi_{\parallel}$ from theory derived by Le et al. (2010). The acceleration of electrons due to a potential difference is similar to what has been observed inside the ion diffusion regions at the magnetopause and magnetotail. The different cases from the magnetopause, magnetotail, and magnetosheath show a good agreement of $\Delta\Phi_{\parallel}/T_{e,\infty}$ scaling with the inflow electron beta, where $T_{e,\infty}$ is the inflow electron temperature (Table 10.3). Furthermore, the different cases show that the local parallel electron temperature increase is a fraction of $\Delta\Phi_{\parallel}$ (Table 10.3). Thus, a similar acceleration mechanism is occurring in all these plasma regions despite their different plasma conditions.

Table 10.1. *Parameters from ion diffusion crossings in the magnetopause (Graham et al., 2016a), magnetotail (Øieroset et al., 2002; Egedal et al., 2005), and magnetosheath (Eriksson et al., 2018), where SL and SR refers to the separatrix regions on the left and right side of the current sheet center, respectively.*

	Magnetopause	Magnetosheath	Magnetotail
$\Delta\Phi_{\parallel}$ (V)	180	58 (SL), 20 (SR)	1000
ΔT_e (eV)	65	18 (SL), 7 (SR)	300
$\Delta e\Phi_{\parallel}/k_b T_{e,\infty}$	3.6	1.38 (SL), 0.47 (SR)	2.5
$\beta_{e,\infty}$	0.01	0.38 (SL) 0.59 (SR)	0.15

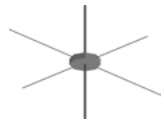

10.4 Summary of Article IV

Electron acceleration in a magnetotail reconnection outflow region using Magnetospheric MultiScale data

Authors
E. Eriksson, A. Vaivads, L. Alm, D. B. Graham,
Yu. V. Khotyaintsev, and M. André

Details
Manuscript in preparation

My Contribution so far
I planned the study, performed the data analysis, and has the main responsibility of writing the article.

Summary

In Article IV we present observations inside a reconnection outflow region located in the magnetotail. Efficient energy conversion takes place in outflow regions of reconnection energizing both ions and electrons. Thus, it is important to understand how particles are accelerated in the outflow regions. In particular, electrons since most of our knowledge from other astrophysical environments comes from electromagnetic radiation generated by accelerated electrons. Inside the outflow region we estimate the power density (W) due to three fundamental electron acceleration mechanisms: Fermi acceleration, betatron acceleration, and acceleration due to a parallel electric field using a guiding-center approximation. To our knowledge these separate terms have not been estimated from reconnection observations before.

We analyze in detail the electron acceleration for an event that has one of the highest power density in the observed outflow region. Figure 10.5 show some observation from that event. During the event $B_x = 0$ is crossed three times (magenta dashed lines), suggesting that MMS crosses the center of the current sheet center three times. V_{ix} is the largest component showing a steady, large, negative flow for the entire event, suggesting that MMS are crossing an outflow region with a tailward flow. During the event the electron temperature varies about 800 eV. The largest peaks in power density are observed in W_{Fermi} in the center of the current sheet. The largest average value for the whole outflow region are also observed in W_{Fermi}, suggesting that Fermi acceleration is the dominant electron acceleration mechanism. In the center of the current

sheet $W_{Betatron}$ also show positive peaks. Each positive peak of $W_{Betatron}$ is surrounded by regions of negative $W_{Betatron}$. On average, $W_{Betatron}$ is near zero slightly negative. $W_{E_{||}}$ (black line) has the smallest power density of all the terms. However, all $W_{E_{||}}$ values has a smaller magnitude than the observational uncertainty levels (yellow shaded area), caused by the uncertainties in the parallel electric field measurements. Thus, it is impossible to draw any further conclusions regarding $W_{E_{||}}$. Most of the observations in Figure 10.5 are consistent with electron acceleration in a simplified sketch of a 2-D reconnection outflow region shown in Figure 7.9f, where spacecraft trajectory is indicated by the green line. In such a simplified sketch, we expect that electrons accelerated by Fermi acceleration should be observed in antiparallel (parallel) direction at $B_x > 0$ ($B_x < 0$). The observations (Figure 10.5h) are consistent with this. In the middle of the current sheet we expect $W_{Betatron} > 0$ and consistent with this we observe an increase in the perpendicular electron flux (Figure 10.5h) around the peak values of $W_{Betatron}$. We expect to see the highest $W_{E_{||}}$ near the separatrix regions, accelerating the thermal electrons moving towards the X-line center. Our observations of parallel (antiparallel) thermal electron beams (Figure 10.5g) at $B_x > 0$ ($B_x < 0$) is consistent with this, however, due to the observational uncertainties in the parallel electric field we cannot make any direct comparisons between $W_{E_{||}}$ and the observed beams.

During the event we also observe a significant change in the power densities, due to Fermi and betatron acceleration, between the first and last current sheet crossing. This suggests that there is a significant complexity in the spatial/temporal evolution of the current sheet that cannot be described by a simple sketch. We also estimate how much energy a thermal electron will gain if it is accelerated by Fermi acceleration for one pass of the current sheet. We find that the estimated energy gain (500 eV) is of the same order as the variations in the temperature. We conclude that Fermi acceleration is the dominant electron acceleration mechanism. More observational and simulation studies are needed to sort out the relative importance of the acceleration mechanisms.

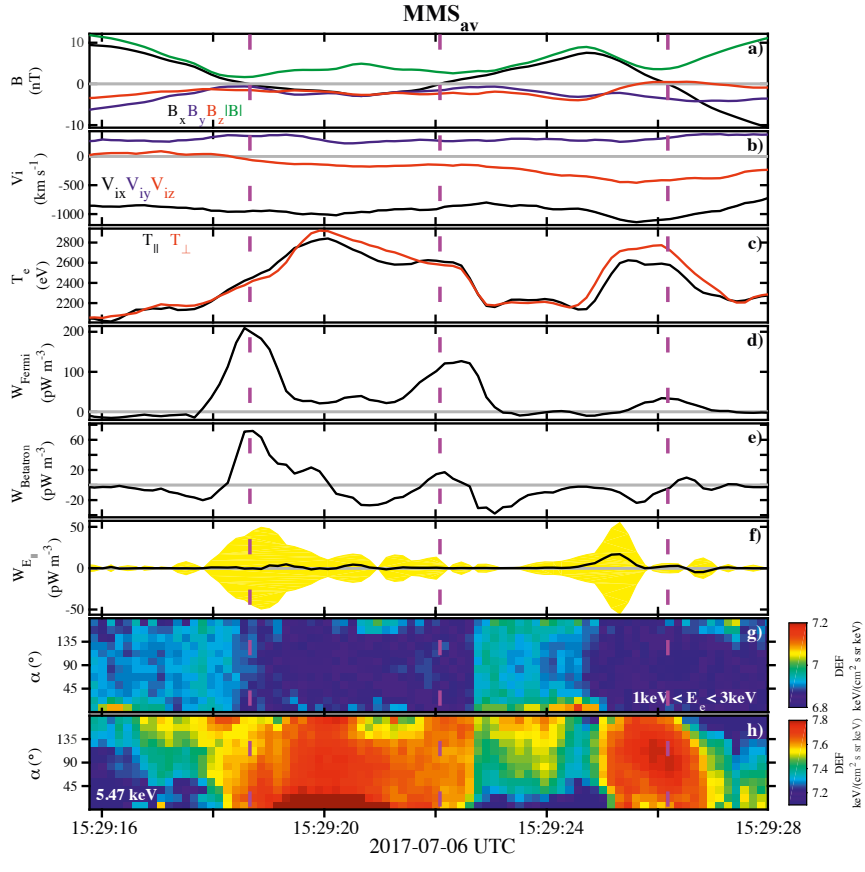

Figure 10.5. Detailed observations from the tailward outflow region studied in Article IV (adapted version). a) the magnetic field, b) ion velocity, c) electron temperature parallel (black line) and perpendicular (red line) to the magnetic field, d)-f) show the electron power density due to d) Fermi acceleration, e) betatron acceleration, f) acceleration by a parallel electric field, where the yellow shaded region indicate the observational uncertainties in $W_{E_{||}}$, g-h) electron pitch angle distribution at g) 1 to 3 keV, h) 5.47 keV. The dashed magenta lines indicate the the current sheet center.

11. Sammanfattning på svenska

Plasma är en gas som består av laddade partiklar och finns överallt i Universum. Ett exempel är rymden kring jorden (några tusen kilometer ovanför jordytan) där jordens magnetfält styr hur de laddade partiklarna rör sig – jordens magnetosfär. Uppvärmning av plasma och acceleration av de laddade partiklarna i plasmat har observerats på många olika ställen i Universum som t.ex. jorden, solen, Jupiter, Saturnus, Merkurius, och vid stjärnor. Hur och vart uppvärmningen och accelerationen sker är fortfarande inte förklarat. I de flesta områden i Universum innehåller plasma negativt laddade elektroner och positivt laddade joner. I denna avhandling fokuserar vi på elektroner. Observationer från utbrott på solen och rester från supernovaexplosioner kommer huvudsakligen från strålning genererad av accelererade elektroner. Därför kan förståelse av elektronacceleration i jordens magnetosfär hjälpa till att förklara vad som händer på andra ställen i Universum. Electronacceleration och uppvärmningsprocesser sker på små längdskalor – skalor där detaljer kring de laddade partiklarnas rörelse är viktig. I jordens magnetosfär är dessa små längdskalor några kilometer. Vi behöver därför detaljerade mätningar av de elektriska och magnetiska fälten samt elektronernas rörelse för att kunna förstå elektroners uppvärmning och acceleration. Elektronacceleration i jordens magnetfält och vid andra planeter som Saturnus, Merkurius, och Jupiter har observerat av satelliter. Flera viktiga plasmaprocesser har studerats tidigare för att försöka förklara den observerade accelerationen som tunna skikt av stark ström, turbulens, och chockvågor. Exakt vilka uppvärmnings- och accelerationsmekanismer som är inblandade och hur viktiga de är, är i många fall inte förklarat. Resultaten i denna avhandling bidrar till en bättre förståelse av detta ämne.

I största delen av Universum rör sig laddade partiklar i plasma med magnetfältet, de sägs vara "infrusna". En fundamental plasmaprocess som ändrar magnetfältets topologi, bryter denna infrysning, och omvandlar magnetisk energi till värme och kinetisk energi är *magnetisk omvandling* (på engelska "magnetic reconnection"). Magnetiska nollpunkter, strukturer där magnetfältet går mot noll, anses vara viktiga i 3-D magnetisk omvandling. Magnetisk omvandling är speciellt intressant att studera eftersom den leder till en storskalig omvandling av magnetfältets geometri och kan leda till att partiklar från solen kan ta sig in i en planets magnetosfär som t.ex. jorden. Den största förändringen av magnetfältet sker i små områden där joner och elektroner bryter från magnetfältet, så kallade diffusionsområden. På större skalor, bildar magnetisk omvandling ett stort flöde av plasma. Energiomvandlingen är väldigt effektiv där detta flöde

genereras, i de så kallade *utflödesområdena* (på engelska "outflow regions"). Elektronacceleration relaterad till magnetisk omvandling har observerats på plats i rymden runt jorden och indirekt med teleskop vid solen. Flera förslag på viktiga accelerationsplatser har getts. Hur viktig dessa platser är i ett större sammanhang är fortfarande inte förklarat. I denna avhandling studerar vi magnetiska nollpunkter och elektronacceleration- och uppvärmningsmekanismer (i två olika områden) i rymden flera tusen kilometer ovanför jordytan med NASA's fyra MMS-satelliter (Artikel II-IV) och ESA's fyra Cluster-satelliter (Artikel I).

I Artikel I presenterar vi en statistisk studie av magnetiska nollpunkter utförd i delen av jordens magnetosfär som är riktat bort från solen - nattsidan. Vi ser att magnetiska nollpunkter är väldigt vanlig på nattsidan och att beskrivningen av magnetfältets geometri runt nollpunkter är känslig mot lokala förändringar i magnetfältet som t.ex. elektromagnetiska vågor. Vi har därför skapat en metod i Artikel I som kan användas för att bestämma om beskrivningen av magnetfältetstopologi runt nollpunkten är påverkad av lokala förändringar i magnetfältet eller inte. Det är viktigt att ha en korrekt beskrivning av magnetfältetstopologi runt nollpunkten eftersom topologin styr plasmaprocesser vid nollpunkten.

I Artikeln II presenterar vi observationer från ett tunt (några km) skikt av stark ström, ett så kallat strömskikt, i det turbulenta området direkt innanför jordens chockvåg. Jordens chockvåg är en kollisonschockvåg som uppstår framför magnetosfären genom samverkan mellan partiklarna och magnetfältet som flödar från solen och jordens magnetosfär. I det turbulenta området direkt innanför jordens chockvåg kan elektroner effektivt värmas upp och accelereras. I strömskiktet i Artikel II såg vi inga tydliga tecken på pågående magnetisk omvandling. Däremot, så observerade vi att elektroner värms upp och att ett elektronflöde parallellt till magnetfältet bildas från en potentialskillnad. Detta elektronflöde har tidigare ansetts bildas enbart vid chockvågen, men i denna artikel visar vi att det också kan bildas innanför chockvågen.

I Artikel III presenterar vi observationer från ett väldigt tunt strömskikt (ännu tunnare än i Artikel II) i det turbulenta området innanför jordens chockvåg. I detta strömskikt såg vi en hel del tecken som tyder på en pågående magnetisk omvandling. Vi observerar också lokal uppvärmning och acceleration av elektroner som rör sig längst magnetfältet mot centrum av magnetiska omvandlingsprocessen. Vi visar i Artikel III att denna uppvärmning och acceleration sker p.g.a. en potentialskillnad istället för elektrostatiska vågor. Liknande uppvärmning- och accelerationsmekanism av elektroner har observerats i andra områden i jordens magnetosfär, trots deras olika plasmamiljöer.

I Artikel IV studerar vi hur mycket energi som överförs till elektroner på grund av tre fundamentala accelerationsmekanismer: Fermiacceleration, betatronacceleration och acceleration p.g.a. parallella elektriska fält i ett utflödesområde på nattsidan. Vi visar att de flesta av observationer överensstämmer med en förenklad 2-D bild av Fermi- och betatronacceleration i ett utflödesområde. Vi konstaterar att den dominanta accelerationsmekanismen är Fer-

miacceleration och rekommenderar att fler observationsstudier och numeriska simuleringar görs för att bättre kunna reda ut hur viktig olika accelerationsmekanismer är.

12. Acknowledgments

As you might have guessed after reading this thesis, understanding space physics is a very intricate and complex task that is defiantly not something one person can do alone. Thus, it should not come as a surprise that this thesis was not possible without the help and support from a lot of other people.

First, I would like to thank my main supervisor Andris Vaivads. This thesis would not be possible without your help, guidance, and easy way of sharing your scientific knowledge. No matter how busy you were you always took the time to answer my questions and was quick to make drawings to help me visualize it. Thank you for involving me in different ISSI groups and allowing me to travel and go to conferences to present my work. For helping me evolve not just as a scientist but as a person. I am very lucky to have had you as my supervisor.

I would also like to thank my co-supervisor Yuri Khotyaintsev for his great advice on how to improve my articles and asking complex questions on my research. If no one questions it, it cannot be improved. I also have to thank my other co-supervisor Stefano Markidis for helping me put my PhD into perspective and understand how simulations works. Without your help I would not have been able to do comparative studies between observations and simulations. A special thank you to Daniel Graham for being my go-to wave expert, helping me understand the complex topic of wave physics and for proof reading my English grammar. I would also like to thank Mats André for always asking me about the bigger context of my work.

A big thanks to everyone at IRF for the friendly and helpful work environment. I never felt unwelcome or stupid when I had a question.

Thanks to Andreas Johlander for always being there when I needed to discuss something. I hope you catch them all! Also my thesis would not look as awesome if you had not created the MMS matlab model. Special thanks to Cecilia Norgren for being there for me when I had questions regarding everything from research to the future. Lots of hugs to all PhD students for all the great moments and laughter.

Thanks to all the instrument teams on Cluster and MMS for all the hard work on both creating the instruments and the ground calibrations.

Last, but not least, I want to thank my parents Kerstin and Per Ola, and my big sister Johanna. Without your support I would not be here today. I cannot thank you enough for everything you have done for me. *Thank you!*

13. Abbreviations

AFG **A**nalog **F**lux**G**ate

DES **D**ual **E**lectron **S**pectrometer

DFG **D**igital **F**lux**G**ate

DIS **D**ual **I**on **S**pectrometer

DSN **D**eep **S**pace **N**etwork

EDP **E**lectric Field **D**ouble **P**robes

EDR **E**lectron **D**iffusion **R**egion

ESA **E**uropean **S**pace **A**gency

FGM **F**lux**G**ate **M**agnetometer

FPI **F**ast **P**lasma **I**nvestigation

GSE **G**eocentric **S**olar **E**cliptic

GSM **G**eocentric **S**olar **M**agnetospheric

IMF **I**nterplanetary **M**agnetic **F**ield

MMS **M**agnetospheric **M**ulti**S**cale

MVA **M**inimum **V**ariance **A**nalysis

NASA **N**ational **A**eronautics and **S**pace **A**dministration

PI **P**oincaré **I**ndex

SCM **S**earch-**C**oil **M**agnetometer

SITL **S**cientist-**I**n-**T**he-**L**oop

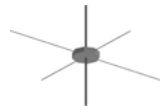

SL **L**eft **S**eparatrix Region

SR **R**ight **S**eparatrix Region

TE **T**aylor **E**xpansion

UTC **C**oordinated **U**niversal **T**ime

UV **U**ltra-**V**iolet

List of Symbols

$E_{\parallel}$	Electric field parallel to the magnetic field
L	Characteristic separation between spacecraft
U	Total kinetic energy density of electrons
V_A	Alfvén speed
V_n	Normal speed of a boundary
W	Work
$\Delta\Phi_{\parallel}$	Potential difference along a magnetic field line
$\Delta\gamma$	Phase difference of a wave
ΔE	Energy change
α	Pitch angle,the angle between the magnetic field and the electron velocity
β	Plasma beta
$\boldsymbol{\kappa}$	Magnetic field curvature vector
δB_1	Minimum disturbance required to alter null type to/from a spiral type
δB_2	Minimum disturbance required to alter null type between A/As and B/BS
ϵ_0	Vacuum permittivity
$\hat{\mathbf{n}}$	Normal direction of a boundary
λ	Eigenvalue
$\mathbf{B}$	Magnetic field
$\mathbf{E}$	Electric field
$\mathbf{F}_L$	Lorentz force
$\mathbf{F}$	Force
$\mathbf{J}$	Total current density
$\mathbf{S}$	Poynting vector
$\mathbf{V}_{\text{field}}$	Velocity of a convecting field line
$\mathbf{dS}_{i,j}$	Relative position between spacecraft i and j
$\mathbf{r}_n$	Position of a magnetic null
$\mathbf{r}$	Position
$\mathbf{u_e}$	Electron bulk velocity
$\mathbf{u_i}$	Ion bulk velocity
$\mathbf{u}_E$	E cross B velocity
$\mathbf{u}$	Bulk flow velocity
$\mathbf{v}_{\text{ph}}$	Wave phase velocity
$\mathbf{v}$	Velocity
As	A 3-D magnetic null type
A	A 3-D magnetic null type
Bs	A 3-D magnetic null type
B	A 3-D magnetic null type
E	Energy

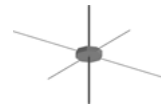

P_{dyn}	Local dynamic pressure
P	Pressure
Re	Earth radius
T	Temperature
V_{shear}	Velocity shear
$W_{Betatron}$	Power density due to betatron acceleration
$W_{E_\parallel}$	Power density due acceleration by a parallel electric field
W_{Fermi}	Power density due to Fermi acceleration
$\nabla\mathbf{B}$	Gradient of the magnetic field
d_e	Electron inertial length
d_i	Ion inertial length
$f(\mathbf{r}, \mathbf{v}, t)$	Particle distribution function (phase space density)
μ_0	Permittivity of free space
μ	First adiabatic invariant, magnetic moment
ω_{pe}	Electron plasma frequency
ω_{pi}	Ion plasma frequency
ρ	Total charge density
σ	Conductivity
J	Second adiabatic invariant
t	Time
θ	Angle between an electric field probe and the magnetic field
$\varepsilon_\perp$	Perpendicular energy
c	Speed of light
$dt_{i,j}$	Time difference between spacecraft i and j
d	Distance between two electric field measurements
e	Elementary charge
f	Frequency
$j_\parallel$	Current parallel to a null's spine
$j_\perp$	Current perpendicular to a null's spine
j_{th}	Threshold current defined in Parnell et al. (1996)
k_b	Boltzmann constant
$k_\parallel$	Wave number parallel to the magnetic field
l	Total length of the magnetic field between two mirror points
m	Mass
n	Number density
$p_\parallel$	Electron pressure parallel to the magnetic field
$p_\perp$	Electron pressure perpendicular to the magnetic field
p	Describes the potential part of the topology of a magnetic null
q	Describes the potential part of the topology of a magnetic null
r_g	A particle's gyroradius
s	Scaling parameter to null method
$u_\parallel$	Electron bulk velocity parallel to the magnetic field
$v_\perp$	Constant speed in the plane perpendicular to the magnetic field

Bibliography

Arridge, C. S. et al. (2016). "Cassini in situ observations of long-duration magnetic reconnection in Saturns magnetotail". *Nature Physics* 12. DOI: 10.1038/nphys3565 (Cited on pages 1, 14).

Baumjohann, W. and R. A. Treumann (1996). *Basic space plasma physics*. London: Imperial College Press. ISBN: 186094079X (Cited on pages 4, 11).

Bellan, P. M. (2006). *Fundamentals of Plasma Physics*. Cambridge. DOI: 10.1007/978-3-642-33848-9 (Cited on page 4).

Benz, A. O. (2016). "Flare Observations". *Living Reviews in Solar Physics* 14. DOI: 10.1007/s41116-016-0004-3 (Cited on pages 44, 46, 47).

Birn, J. and E. R. Priest (2007). *Reconnection of Magnetic Fields*. Cambridge: Cambridge University Press. ISBN: 0521854202. DOI: 10.1017/CBO9780511536151 (Cited on pages 1, 14, 16, 53).

Birn, J. et al. (2012). "Particle Acceleration in the Magnetotail and Aurora". *Space Science Review* 173. DOI: 10.1007/s11214-012-9874-4 (Cited on pages 1, 2, 41, 44, 46, 47).

Birn, J. et al. (2013). "Particle acceleration in dipolarization events". *Journal of Geophysical Research: Space Physics* 118. DOI: 10.1002/jgra.50132 (Cited on pages 1, 41, 44).

Burch, J. L. et al. (2016). "Magnetospheric Multiscale Overview and Science Objectives". *Space Science Reviews* 199. DOI: 10.1007/s11214-015-0164-9 (Cited on pages 20, 21).

Cairns, Iver H. and B. F. McMillan (2005). "Electron acceleration by lower hybrid waves in magnetic reconnection regions". *Physics of Plasmas* 12. DOI: 10.1063/1.2080567 (Cited on page 1).

Cargill, P. J. et al. (2012). "Current Fragmentation and Particle Acceleration in Solar Flares". *Space Science Reviews* 173. DOI: 10.1007/s11214-012-9888-y (Cited on page 2).

Chanteur, G. (1998). "Spatial Interpolation for Four Spacecraft: Theory". In: *Analysis Methods for Multi-Spacecraft Data*. Ed. by Götz Paschmann and Patrick Daly. ESA/ISSI, pp. 349–370. ISBN: 1608-280X (Cited on page 27).

Chasapis, A. et al. (2015). "Thin Current Sheets and Associated Electron Heating in Turbulent Space Plasma". *The Astrophysical Journal* 804. DOI: 10.1088/2041-8205/804/1/L1 (Cited on pages 12, 55).

Chasapis, A. et al. (2017). "Electron Heating at Kinetic Scales in Magnetosheath Turbulence". *The Astrophysical Journal* 836. DOI: 10.3847/1538-4357/836/2/247 (Cited on page 49).

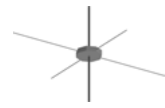

Chen, B. et al. (2015). "Particle acceleration by a solar flare termination shock". *Science* 350.
DOI: 10.1126/science.aac8467 (Cited on page 1).

Chen, F. F. (1974). *Introduction to Plasma Physics and Controlled Fusion Plasma Physics*. New York.
DOI: 10.1063/1.2814568 (Cited on page 4).

Chen, L. et al. (2008). "Observation of energetic electrons within magnetic islands". *Nature Physics* 4.
DOI: 10.1038/nphys777 (Cited on page 1).

Chen, Y. et al. (2016). "Imaging a Magnetic-breakout Solar Eruption". *The Astrophysical Journal* 820.
DOI: 10.3847/2041-8205/820/2/L37 (Cited on page 16).

Chernyshov, D. et al. (2017). "Fermi bubbles as sources of cosmic rays above 1 PeV". *EPJ Web Conference* 145.
DOI: 10.1051/epjconf/201614504004 (Cited on page 44).

Cowley, S. W. H. (1973). "A qualitative study of the reconnection between the Earth's magnetic field and an interplanetary field of arbitrary orientation". *Radio Science* 8.
DOI: 10.1029/RS008i011p00903 (Cited on pages 16, 17).

Cowley, S. W. H. and C. J. Owen (1989). "A simple illustrative model of open flux tube motion over the dayside magnetopause". *Planetary and Space Science* 37.
DOI: 10.1016/0032-0633(89)90116-5 (Cited on page 14).

Dahlin, J. T. et al. (2014). "The mechanisms of electron heating and acceleration during magnetic reconnection". *Physics of Plasmas* 21.
DOI: 10.1063/1.4894484 (Cited on page 36).

Dahlin, J. T. et al. (2016). "Parallel electric fields are inefficient drivers of energetic electrons in magnetic reconnection". *Physics of Plasmas* 23.
DOI: 10.1063/1.4972082 (Cited on page 44).

Dandouras, I. et al. (2010). "Cluster Ion Spectrometry (CIS) Data in the Cluster Active Archive (CAA)". In: *The Cluster Active Archive*. Ed. by Harri Laakso et al. Dordrecht: Springer Netherlands, pp. 51–72. ISBN: 978-90-481-3499-1 (Cited on page 23).

Deng, X. H. et al. (2009). "Dynamics and waves near multiple magnetic null points in reconnection diffusion region". *Journal of Geophysical Research: Space Physics* 114.
DOI: 10.1029/2008JA013197 (Cited on page 16).

Dewey, R. M. et al. (2017). "Energetic Electron Acceleration and Injection During Dipolarization Events in Mercury's Magnetotail". *Journal of Geophysical Research: Space Physics* 122.
DOI: 10.1002/2017JA024617 (Cited on pages 1, 41, 44).

Doss, C. E. et al. (2015). "Asymmetric magnetic reconnection with a flow shear and applications to the magnetopause". *Journal of Geophysical Research:*

Space Physics.
DOI: 10.1002/2015JA021489 (Cited on page 14).

Doss, C. E. et al. (2016). "Particle-in-cell simulation study of the scaling of asymmetric magnetic reconnection with in-plane flow shear". *Physics of Plasmas* 23.
DOI: 10.1063/1.4960324 (Cited on page 14).

Drake, J. F. et al. (2006). "Electron acceleration from contracting magnetic islands during reconnection". *Nature* 443.
DOI: 10.1038/nature05116 (Cited on page 2).

Drake, J. F. et al. (2013). "The Power-law Spectra of Energetic Particles during Multi-island Magnetic Reconnection". *The Astrophysical Journal Letters* 763.
DOI: 10.1088/2041-8205/763/1/L5 (Cited on page 2).

Egedal, J. et al. (2005). "In Situ Discovery of an Electrostatic Potential, Trapping Electrons and Mediating Fast Reconnection in the Earth's Magnetotail". *Physical Review Letters* 94.
DOI: 10.1103/PhysRevLett.94.025006 (Cited on page 60).

Egedal, J. et al. (2007). "Laboratory Observations of Spontaneous Magnetic Reconnection". *Physical Review Letters* 98.
DOI: 10.1103/PhysRevLett.98.015003 (Cited on page 1).

Ergun, R. E. et al. (2016). "The Axial Double Probe and Fields Signal Processing for the MMS Mission". *Space Science Reviews* 199.
DOI: 10.1007/s11214-014-0115-x (Cited on page 23).

Eriksson, E. et al. (2015). "Statistics and accuracy of magnetic null identification in multispacecraft data". *Geophysical Research Letters* 42.
DOI: 10.1002/2015GL064959 (Cited on pages 52, 54).

Eriksson, E. et al. (2016). "Strong current sheet at a magnetosheath jet: Kinetic structure and electron acceleration". *Journal of Geophysical Research: Space Physics* 121.
DOI: 10.1002/2016JA023146 (Cited on pages 8, 41, 56).

Eriksson, E. et al. (2018). "Electron energization at a reconnecting magnetosheath current sheet". *Geophysical Research Letters* 45.
DOI: 10.1029/2018GL078660 (Cited on pages 30, 34, 35, 46, 59, 60).

Escoubet, C. P. et al. (2001). "Introduction The Cluster mission". *Annales Geophysicae* 19.
DOI: 10.5194/angeo-19-1197-2001 (Cited on page 19).

Escoubet, C. P. et al. (2013). "Dynamical processes in space: Cluster results". *Annales Geophysicae* 31.
DOI: 10.5194/angeo-31-1045-2013 (Cited on page 19).

Fazakerley, A. N. et al. (2010). "PEACE Data in the Cluster Active Archive". In: *The Cluster Active Archive*. Ed. by Harri Laakso et al. Dordrecht: Springer Netherlands, pp. 129–144. ISBN: 978-90-481-3499-1 (Cited on page 23).

Feldman, W. C. et al. (1983). "Electron velocity distributions near the earth's bow shock". *Journal of Geophysical Research* 88.
DOI: 10.1029/JA088iA01p00096 (Cited on pages 1, 39, 46, 57).

Freed, M. S. et al. (2015). "Three-Year Global Survey of Coronal Null Points from Potential-Field-Source-Surface (PFSS) Modeling and Solar Dynamics Observatory (SDO) Observations". *Solar Physics* 290.
DOI: 10.1007/s11207-014-0616-5 (Cited on page 16).

Fu, H. S. et al. (2011). "Fermi and betatron acceleration of suprathermal electrons behind dipolarization fronts". *Geophysical Research Letters* 38.
DOI: 10.1029/2011GL048528 (Cited on pages 1, 41, 43).

Fu, H. S. et al. (2013). "Energetic electron acceleration by unsteady magnetic reconnection". *Nature Physics* 9.
DOI: 10.1038/nphys2664 (Cited on page 2).

Fu, H. S. et al. (2015). "How to find magnetic nulls and reconstruct field topology with MMS data?" *Journal of Geophysical Research: Space Physics* 120.
DOI: 10.1002/2015JA021082 (Cited on page 26).

Fu, H. S. et al. (2016). "Identifying magnetic reconnection events using the FOTE method". 121.
DOI: 10.1002/2015JA021701 (Cited on page 26).

Fu, H. S. et al. (2017). "Intermittent energy dissipation by turbulent reconnection". *Geophysical Research Letters* 44.
DOI: 10.1002/2016GL071787 (Cited on page 49).

Fuselier, S. A. et al. (2016). "Magnetospheric Multiscale Science Mission Profile and Operations". *Space Science Reviews* 199.
DOI: 10.1007/s11214-014-0087-x (Cited on page 21).

Gloag, J. M. et al. (2010). "FGM Data Products in the CAA". In: *The Cluster Active Archive*. Ed. by Harri Laakso et al. Dordrecht: Springer Netherlands, pp. 109–128. ISBN: 978-90-481-3499-1 (Cited on page 20).

Gosling, J. T. et al. (2005). "Absence of energetic particle effects associated with magnetic reconnection exhausts in the solar wind". *Geophysical Research Letters* 32.
DOI: 10.1029/2005GL023357 (Cited on page 14).

Graham, D. B. et al. (2014). "Electron Dynamics in the Diffusion Region of an Asymmetric Magnetic Reconnection". *Physical Review Letters* 112.
DOI: 10.1103/PhysRevLett.112.215004 (Cited on pages 1, 46).

Graham, D. B. et al. (2016a). "Electron currents and heating in the ion diffusion region of asymmetric reconnection". *Geophysical Research Letters* 43.
DOI: 10.1002/2016GL068613 (Cited on pages 46, 60).

Graham, D. B. et al. (2016b). "Electrostatic solitary waves and electrostatic waves at the magnetopause". *Journal of Geophysical Research: Space Physics* 121.
DOI: 10.1002/2015JA021527 (Cited on page 34).

Greene, J. M. (1988). "Geometrical Properties of Three-Dimensional Reconnecting Magnetic Fields With Nulls". *Journal of Geophysical Research* 93. DOI: 10.1029/JA093iA08p08583 (Cited on page 17).

Greene, J. M. (1992). "Locating Three- Dimensional Roots by a Bisection Method *". *Journal of Computational Physics* 98. DOI: 10.1016/0021-9991(92)90137-N (Cited on page 26).

Hao, Y. et al. (2016). "Formation of downstream high-speed jets by a rippled nonstationary quasi-parallel shock: 2-D hybrid simulations". *Journal of Geophysical Research: Space Physics* 121. DOI: 10.1002/2015JA021419 (Cited on page 55).

Hasegawa, H. et al. (2007). "Reconstruction of a bipolar magnetic signature in an earthward jet in the tail: Flux rope or 3D guide-field reconnection?" *Journal of Geophysical Research: Space Physics* 112. DOI: 10.1029/2007JA012492 (Cited on page 14).

He, J.-S. et al. (2008). "A magnetic null geometry reconstructed from Cluster spacecraft observations". *Journal of Geophysical Research: Space Physics* 113. DOI: 10.1029/2007JA012609 (Cited on page 16).

Helder, E. A. et al. (2012). "Observational Signatures of Particle Acceleration in Supernova Remnants". *Space Science Reviews* 173. DOI: 10.1007/s11214-012-9919-8 (Cited on page 1).

Hietala, H. et al. (2009). "Supermagnetosonic jets behind a collisionless quasi-parallel shock". *Physical Review Letters* 103. DOI: 10.1103/PhysRevLett.103.245001 (Cited on page 55).

Hong, J. et al. (2016). "Bidirectional Outflows as Evidence of Magnetic Reconnection Leading to a Solar Microflare". *The Astrophysical Journal Letters* 820. DOI: 10.3847/2041-8205/820/1/L17 (Cited on page 14).

Hoshino, M. (2012). "Stochastic Particle Acceleration in Multiple Magnetic Islands during Reconnection". *Physical Review Letters* 108. DOI: 10.1103/PhysRevLett.108.135003 (Cited on page 2).

Hoshino, M. et al. (2001). "Suprathermal electron acceleration in magnetic reconnection". *Journal of Geophysical Research* 106. DOI: 10.1029/2001JA900052 (Cited on page 2).

Jovanovic, D. et al. (2005). "Magnetic reconnection on the ion-skin-depth scale in the dusty magnetotail of a comet". *Physics of Plasmas* 12. DOI: 10.1063/1.1883184 (Cited on pages 1, 14).

Kallenrode, M-B (2010). *Space Physics An Introduction to Plasmas and Particles in the Heliosphere and Magnetospheres*. 3rd ed. Berlin: Springer-Verlag. ISBN: 3-540-206 (Cited on page 4).

Karimabadi, H. et al. (2014). "The link between shocks, turbulence, and magnetic reconnection in collisionless plasmas". *Physics of Plasmas* 21. DOI: 10.1063/1.4882875 (Cited on pages 12, 55).

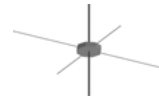

Khotyaintsev, Yu. V. et al. (2011). "Plasma jet braking: Energy dissipation and nonadiabatic electrons". *Physical Review Letters* 106.
DOI: 10.1103/PhysRevLett.106.165001 (Cited on page 41).

Kivelson, M. G. and C. T. Russell (1996). *Introduction to Space Physics*. Cambridge: Cambridge University Press.
DOI: 10.1119/1.2201848 (Cited on pages 4, 11).

Lau, Y-T. and J. M. Finn (1990). "Three-Dimensional kinematic reconnection in the presence of field nulls and closed field lines". *The Astrophysical Journal* 350.
DOI: 10.1086/168419 (Cited on pages 16, 17).

Le Contel, O. et al. (2016). "The Search-Coil Magnetometer for MMS". *Space Science Reviews* 199.
DOI: 10.1007/s11214-014-0096-9 (Cited on pages 23, 24).

Le, A. et al. (2010). "Magnitude of the Hall fields during magnetic reconnection". *Geophysical Research Letters* 37.
DOI: 10.1029/2009GL041941 (Cited on page 60).

Lindqvist, P.-A. et al. (2016). "The Spin-Plane Double Probe Electric Field Instrument for MMS". *Space Science Reviews* 199.
DOI: 10.1007/s11214-014-0116-9 (Cited on page 23).

Lynch, B. J. et al. (2008). "Topological Evolution of a Fast Magnetic Breakout CME in Three Dimensions". *The Astrophysical Journal* 683.
DOI: 10.1086/589738 (Cited on page 16).

Masters, A. et al. (2016). "Suprathermal Electrons at Saturn's Bow Shock". *The Astrophysical Journal* 826.
DOI: 10.3847/0004-637X/826/1/48 (Cited on pages 1, 47).

Mauk, B. H. et al. (2017). "Discrete and broadband electron acceleration in Jupiter's powerful aurora". *Nature* 549.
DOI: 10.1038/nature23648 (Cited on pages 1, 47).

Mitchell, J. J. and S. J. Schwartz (2013). "Nonlocal electron heating at the Earth's bow shock and the role of the magnetically tangent point". *Journal of Geophysical Research: Space Physics* 118.
DOI: 10.1002/2013JA019226 (Cited on page 57).

Nagai, T. (2006). "Location of magnetic reconnection in the magnetotail". *Space Science Reviews* 122.
DOI: 10.1007/s11214-006-6216-4 (Cited on page 14).

Northrop, T. G. (1963). "Adiabatic charged-particle motion". *Reviews of Geophysics* 1.
DOI: 10.1029/RG001i003p00283 (Cited on page 36).

Øieroset, M. et al. (2002). "Evidence for Electron Acceleration up to ~ 300 keV in the Magnetic Reconnection Diffusion Region of Earth's Magnetotail". *Physical Review Letters* 89.
DOI: 10.1103/PhysRevLett.89.195001 (Cited on page 60).

Oka, M. et al. (2017). "Electron Scattering by High-frequency Whistler Waves at Earth's Bow Shock". *The Astrophysical Journal Letters* 842.
DOI: 10.3847/2041-8213/aa7759 (Cited on page 47).

Olshevsky, V. et al. (2016). "Magnetic Null Points in Kinetic Simulations of Space Plasmas". *The Astrophysical Journal* 819.
DOI: 10.3847/0004-637X/819/1/52 (Cited on page 49).

Omidi, N. et al. (2016). "Impacts of spontaneous hot flow anomalies on the magnetosheath and magnetopause". *Journal of Geophysical Research: Space Physics* 121.
DOI: 10.1002/2015JA022170 (Cited on pages 12, 55).

Parnell, C. E. et al. (1996). "The structure of three-dimensional magnetic neutral points". *Physics of Plasmas* 3.
DOI: 10.1063/1.871810 (Cited on pages 28, 71).

Paschmann, G. et al. (2013). "In-Situ Observations of Reconnection in Space". *Space Science Reviews* 178.
DOI: 10.1007/s11214-012-9957-2 (Cited on page 1).

Petrosian, V. (2016). "Particle Acceleration in Solar Flares and Associated CME Shocks". *The Astrophysical Journal* 830.
DOI: 10.3847/0004-637X/830/1/28 (Cited on page 1).

Phan, T. D. et al. (2007). "Evidence for an elongated (>60 ion skin depths) electron diffusion region during fast magnetic reconnection". *Physical Review Letters* 99.
DOI: 10.1103/PhysRevLett.99.255002 (Cited on page 14).

Phan, T. D. et al. (2018). "Electron magnetic reconnection without ion coupling in Earth's turbulent magnetosheath". *Nature* 557.
DOI: 10.1038/s41586-018-0091-5 (Cited on page 58).

Plaschke, F. et al. (2013). "Anti-sunward high-speed jets in the subsolar magnetosheath". *Annales Geophysicae* 31.
DOI: 10.5194/angeo-31-1877-2013 (Cited on page 12).

Pollock, C. et al. (2016). "Fast Plasma Investigation for Magnetospheric Multiscale". *Space Science Reviews* 199.
DOI: 10.1007/s11214-016-0245-4 (Cited on pages 22, 23).

Priest, E. R. (2003). "On the nature of three-dimensional magnetic reconnection". *Journal of Geophysical Research* 108.
DOI: 10.1029/2002JA009812 (Cited on pages 1, 14).

Priest, E. R. and T. G. Forbes (2000). *Magnetic reconnection: MHD Theory and Applications*. New York: Cambridge University Press. ISBN: 9780521481793.
DOI: 10.1029/EO065i013p00124 (Cited on pages 1, 4, 14, 16).

Pritchett, P. L. (2008). "Energetic electron acceleration during multi-island coalescence". *Physics of Plasmas* 15.
DOI: 10.1063/1.2996321 (Cited on page 2).

Rager, A.C. et al. (2018). "Electron crescent distributions as a manifestation of diamagnetic drift in an electron scale current sheet: Magnetospheric Multiscale observations using new 7.5 ms Fast Plasma Investigation moments".

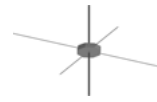

Geophysical Research Letters.
DOI: 10.1002/2017GL076260 (Cited on page 23).

Retinò, A. et al. (2007). "In situ evidence of magnetic reconnection in turbulent plasma". *Nature Physics* 3.
DOI: 10.1038/nphys574 (Cited on pages 12, 14, 55).

Retinò, A. et al. (2008). "Cluster observations of energetic electrons and electromagnetic fields within a reconnecting thin current sheet in the earth's magnetotail". *Journal of Geophysical Research: Space Physics* 113.
DOI: 10.1029/2008JA013511 (Cited on page 1).

Russell, C. T. et al. (2016a). *Space Physics: An Introduction*. Cambridge University Press. ISBN: 9781107098824 (Cited on page 11).

Russell, C. T. et al. (2016b). "The Magnetospheric Multiscale Magnetometers". *Space Science Reviews* 199.
DOI: 10.1007/s11214-014-0057-3 (Cited on page 23).

Schwartz, S. J. (1998). "Shock and Discontinuity Normals, Mach Numbers, and Related Parameters". In: ed. by Götz Paschmann and Patrick Daly. ESA/ISSI, pp. 249–270. ISBN: 1608-280X (Cited on page 31).

Schwartz, S. J. et al. (1998). "Multi-Spacecraft Analysis of Plasma Kinetics". In: *Analysis Methods for Multi-Spacecraft Data*. Ed. by Götz Paschmann and Patrick Daly. ESA/ISSI, pp. 159–184. ISBN: 1608-280X (Cited on page 35).

Sonnerup, B. U. Ö and M. Scheible (1998). "Minimum and maximum variance analysis". In: *Analysis Methods for Multi-Spacecraft Data*. Ed. by Götz Paschmann and Patrick Daly. ESA/ISSI, pp. 185–220. ISBN: 1608-280X (Cited on page 29).

Swanson, D. G. (1989). *Plasma Waves*. Academic Press. ISBN: 0-12-678995-X (Cited on page 47).

Torbert, R. B. et al. (2016). "The FIELDS Instrument Suite on MMS: Scientific Objectives, Measurements, and Data Products". *Space Science Reviews* 199.
DOI: 10.1007/s11214-014-0109-8 (Cited on page 24).

Turner, D. L. et al. (2016). "Energy limits of electron acceleration in the plasma sheet during substorms: A case study with the Magnetospheric Multiscale (MMS) mission". *Geophysical Research Letters* 43.
DOI: 10.1002/2016GL069691 (Cited on pages 1, 41, 44).

Vaivads, A. et al. (2009). "Magnetic reconnection in space plasma". *Plasma Physics and Controlled Fusion* 51.
DOI: 10.1088/0741-3335/51/12/124016 (Cited on page 2).

Watt, C. E. J. and R. Rankin (2008). "Electron acceleration and parallel electric fields due to kinetic Alfvén waves in plasma with similar thermal and Alfvén speeds". *Advances in Space Research* 42.
DOI: 10.1016/j.asr.2007.03.030 (Cited on page 47).

Wendel, D. E. and M. L. Adrian (2013). "Current structure and nonideal behavior at magnetic null points in the turbulent magnetosheath". *Journal*

of Geophysical Research: Space Physics 118.
DOI: 10.1002/jgra.50234 (Cited on page 16).

Wezgowieca, M. et al. (2016). "Hot gas and magnetic arms of NGC 6946: Indications for reconnection heating?" *Astronomy and Astrophysics* 585.
DOI: 10.1051/0004-6361/201526833 (Cited on page 14).

Wilder, F. D. et al. (2018). "The role of the parallel electric field in electron-scale dissipation at reconnecting currents in the magnetosheath". *Journal of Geophysical Research: Space Physics* 123.
DOI: 10.1029/2018JA025529 (Cited on page 50).

Xiao, C. J. et al. (2006). "In situ evidence for the structure of the magnetic null in a 3D reconnection event in the Earth's magnetotail". *Nature Physics* 2.
DOI: 10.1038/nphys342 (Cited on page 16).

Xiao, C. J. et al. (2007). "Satellite observations of separator-line geometry of three-dimensional magnetic reconnection". *Nature Physics* 3.
DOI: 10.1038/nphys650 (Cited on pages 14, 16).

Yamada, M. et al. (2010). "Magnetic reconnection". *Reviews of Modern Physics* 82.
DOI: 10.1103/RevModPhys.82.603 (Cited on page 1).

Zeng, Z. et al. (2016). "Resolving the Fan-spine Reconnection Geometry of a Small-scale Chromospheric Jet Event with the New Solar Telescope". *The Astrophysical Journal* 819.
DOI: 10.3847/2041-8205/819/1/L3 (Cited on page 16).

Acta Universitatis Upsaliensis

Digital Comprehensive Summaries of Uppsala Dissertations from the Faculty of Science and Technology 1719

Editor: The Dean of the Faculty of Science and Technology

A doctoral dissertation from the Faculty of Science and Technology, Uppsala University, is usually a summary of a number of papers. A few copies of the complete dissertation are kept at major Swedish research libraries, while the summary alone is distributed internationally through the series Digital Comprehensive Summaries of Uppsala Dissertations from the Faculty of Science and Technology. (Prior to January, 2005, the series was published under the title "Comprehensive Summaries of Uppsala Dissertations from the Faculty of Science and Technology".)

Distribution: publications.uu.se
urn:nbn:se:uu:diva-359594

ACTA
UNIVERSITATIS
UPSALIENSIS
UPPSALA
2018